



Analysis

<https://doi.org/10.1038/s44220-024-00352-9>

Functional brain network dynamics mediate the relationship between female reproductive aging and interpersonal adversity

Received: 24 February 2024

Accepted: 10 October 2024

Published online: 7 January 2025

Check for updates

Raluca Petrican¹✉, Sidhant Chopra^{1,2,3,4}, Ashlea Segal^{5,6}, Nick Fallon¹ & Alex Fornito⁵

Premature reproductive aging is linked to heightened stress sensitivity and psychological maladjustment across the life course. However, the brain dynamics underlying this relationship are poorly understood. Here, to address this issue, we analyzed multimodal data from female participants in the Adolescent Brain and Cognitive Development (longitudinal, $N=441$; aged 9–12 years) and Human Connectome-Aging (cross-sectional, $N=130$; aged 36–60 years) studies. Age-specific intrinsic functional brain network dynamics mediated the link between reproductive aging and perceptions of greater interpersonal adversity. The adolescent profile overlapped areas of greater glutamatergic and dopaminergic receptor density, and the middle-aged profile was concentrated in visual, attentional and default mode networks. The two profiles showed opposite relationships with patterns of functional neural network variability and cortical atrophy observed in psychosis versus major depressive disorder. Our findings underscore the divergent patterns of brain aging linked to reproductive maturation versus senescence, which may explain developmentally specific vulnerabilities to distinct disorders.

Accelerated reproductive aging is linked to risk for psychopathology across the lifespan^{1–6}. This relationship probably reflects the neuroplastic and stress-modulating effects of gonadal hormones, documented most consistently for biological female organisms^{3,7–9}. Indeed, substantial cross-species evidence suggests that ovarian hormones can counteract hypothalamic–pituitary–adrenal (HPA) axis-evoked neuroplastic processes associated with poorer cognitive performance and psychopathology^{10,11}, including those foreshadowing dementia risk (for example, hippocampal tau accumulation, atrophy and deficient functional connectivity), leading to associative learning and memory deficits^{12–14}.

Although compelling, the evidence considered above comes primarily from the rodent literature and focuses on short-term fluctuations in gonadal hormones. These findings provide only limited insights into the neuroplastic mechanisms underlying the link between stress exposure/susceptibility and faster progression of reproductive maturation (that is, earlier pubertal timing) or senescence (that is, earlier menopausal onset¹⁵). Moreover, in humans, there is compelling evidence of a bidirectional relationship between reproductive aging and stress, as hormonal fluctuations linked to faster progression towards reproductive aging milestones, such as puberty or menopause, enhance stress susceptibility¹⁰, whereas stress exposure accelerates

¹Institute of Population Health, Department of Psychology, University of Liverpool, Liverpool, UK. ²Department of Psychology, Yale University, New Haven, CT, USA. ³Department of Psychiatry, Brain Health Institute, Rutgers University, Piscataway, NJ, USA. ⁴Orygen, Parkville, Victoria, Australia. ⁵School of Psychological Sciences, The Turner Institute for Brain and Mental Health, and Monash Biomedical Imaging, Monash University, Melbourne, Victoria, Australia. ⁶Wu Tsai Institute and Department of Neuroscience, Yale University, New Haven, CT, USA. ✉e-mail: raluca.petrican@liverpool.ac.uk

reproductive aging¹. Although accelerated reproductive aging as a putative marker of greater allostatic load heightens the risk for psychopathology across the life course^{1,16,17}, its immediate adaptive value and brain correlates are likely to vary with age. For instance, in adolescence, accelerated maturation in response to greater ‘wear and tear’ is regarded as an evolutionarily adaptive mechanism because it maximizes the reproductive opportunities for an organism that is likely set for an early demise^{18,19}. To our knowledge, there is no comparable argument on the adaptiveness of accelerated reproductive senescence. In earlier life, the link between reproductive aging and psychopathology is likely to reflect the neuroplastic effects of gonadal hormones, with precocious reproductive maturation hindering the fine-tuning of the slower developing association networks that are transdiagnostically involved in psychopathology^{17,20}. Complementarily, in later adulthood, premature reproductive senescence would deprive individuals of the neuroprotective effects of ovarian hormones, thereby increasing susceptibility to stress and dementia^{9,13}. Understanding the age-specific neurodevelopmental correlates of the relationship between stress and reproductive aging is thus foundational to the design of personalized detection and intervention paradigms intended to alleviate adverse psychological consequences^{21,22}.

To probe this question, we analyzed multimodal data from female participants in the Adolescent Brain and Cognitive Development (ABCD) and Human Connectome Project–Aging (HCP-A) studies. We focused on female participants for two reasons. One was the availability of well-validated measures indexing stages of reproductive aging based on quantifiable factors (for example, reproductive cycle characteristics, gonadal hormone levels). A second reason was the greater susceptibility and exposure to adversity, including pain and hostility from others, observed in female relative to male individuals^{23–25}. Use of the ABCD and HCP-A datasets allowed us to compare two life stages associated with higher stress vulnerability among female individuals^{10,26}, but typified by complementary endocrine contexts (that is, increasing versus decreasing ovarian hormone levels³) and thus, probably, differential capacity to withstand adversity²⁷. In line with prior studies^{1,28,29}, accelerated reproductive aging was estimated separately within each sample as earlier pubertal timing (ABCD) or more advanced menopausal status (HCP-A) relative to other participants of the same chronological age. To operationalize exposure and sensitivity to stress, we examined participants’ experiential ratings of pain and interpersonal adversity (that is, hostility from others), which cross-species research has shown to robustly engage the HPA axis and associated neuroimmune responses^{12,27,30–35}. By focusing on pain and interpersonal adversity as the stressors of interest, we were able to draw direct comparisons between our present study and previous rodent literature in which the inter-relationships among gonadal hormones, stress exposure, neurocognitive functioning, as well as psychopathology-like behaviors, have been studied most extensively.

In previous investigations, accelerated brain development, estimated either longitudinally or cross-sectionally relative to same-chronological-age peers, was independently linked to greater stress exposure/reactivity^{36,37} and faster reproductive maturation^{2,38,39}. However, evidence of its role in mediating the relationship between stress and reproductive aging is lacking, partly due to the fact that most studies have focused on structural markers of neurodevelopment (for example, cortical thickness and gray matter volume (GMV)^{2,4}; but see ref. ⁴⁰ for an exception), which may not be as sensitive as measures of brain function for capturing individual differences in cognition, affect and psychopathology^{41,42}.

We therefore examined two intrinsic (that is, resting state) markers of brain function that reportedly play a key role in adjustment to environmental stressors: variability (that is, within-individual standard deviation) in regional time series (TSV) and moment-to-moment variability of inter-regional functional coupling (FCV). These two markers show divergent associations with measures of adaptive functioning.

Table 1 | Demographic information for the ABCD and HCP-A samples

Variable	ABCDN=441	HCP-AN=130
Age (years) (Time 1/ Time 2 (ABCD))	9.94±0.61/11.94±0.63	47.69±7.00
Handedness ^a	81%	96%
Race ^b	White (100%)	Asian (5%) Black (21%) White (62%) Mixed race (7%) Not reported (5%)
Household income (US\$) ^c	<50,000 (15%) 50,000–74,999 (13.9%) 75,000–99,999 (21.4%) 100,000–199,000 (37%) >200,000 (12.7%)	<50,000 (24.6%) 50,000–74,999 (23.8%) 75,000–99,999 (20%) 100,000–199,000 (23.8%) >200,000 (7.7%)
Traumatic brain injury	0.24±0.53	0.27±0.96
Average motion (mm) ^d	0.16±0.14/0.12±0.09	0.10±0.04

Note. ^aPercent predominantly right-handed. ^bRace was based on parental reports in the ABCD sample and self-reports in the HCP-A sample. ^cAssessed at baseline. ^dTime 1/Time 2 (ABCD).

Specifically, greater TSV is thought to reflect a brain’s wider ‘dynamic range’ and thus its capacity to respond in a more differentiated manner to external stimuli and environmental challenges^{43–46}. FCV has been linked to maladaptive entrainment with the external milieu⁴⁷. Greater intrinsic FCV, broadly operationalized as more frequent moment-to-moment changes in functional coupling strength between a given region and the rest of the brain, is regarded as a marker of brain network architectural instability over time^{48–50}.

The two variability indices show distinguishable trajectories of lifespan development. From childhood to middle adolescence, intrinsic TSV shows regionally specific maturational trajectories that track intracortical myelination patterns (that is, declines in sensory region and increases in transmodal association areas⁵¹). Intrinsic FCV declines steadily with development, as individualized motifs of functional network segregation and integration emerge^{52,53}. From middle adulthood onwards, normative declines in TSV predict longitudinal age-related decrements of cognitive performance⁴³, while advancing age has been associated with rising FCV⁵⁴, which, in turn, foreshadows declining cognitive performance^{48,50,55}.

Our primary objective was to characterize TSV/FCV patterns suggestive of accelerated/decelerated brain aging relative to same-chronological-age peers³⁷ that could explain the previously documented bidirectional relationship between reproductive aging and stress susceptibility^{1,10} (see Table 1 for sample demographics). We defined the latter in reference to the participants’ perceptions of recently experienced pain and exposure to interpersonal adversity. For the adolescent sample of the ABCD Study, the longitudinal design allowed us to investigate the temporal stability of the relationship between brain function and reproductive aging (at Time 1/baseline and Time 2/two-year follow-up, respectively) and the potential prospective prediction of Time 2 measures of pain/hostility from the Time 1 brain measures.

Our second objective was to elucidate the broader functional relevance of variations in reproductive and brain aging. We thus sought to shed light on whether our identified TSV/FCV patterns could be relevant to understanding vulnerability to psychiatric disorders typified by premature neural senescence⁵⁶. To do so, we examined the overlap between the spatial topography of functional brain variability tracking reproductive aging versus symptom severity in two psychiatric disorders associated with accelerated brain aging⁵⁶ and with adolescent onset⁵⁷, psychosis and major depressive disorder (MDD)^{58–62} (see Table 2 for psychiatric sample demographics). Extant evidence suggests that enhanced vulnerability to psychopathology during key female hormonal transitions, such as puberty and menopause, may reflect, at least

Table 2 | Demographic information on the datasets contributing to the FCV and disorder-specific atrophy maps

Controls				Patients		
Disorder group	No. of subjects (% male, % female)	Age range	Race (%)	No. of subjects (% male, % female)	Age range (years)	Race (%)
MDD ¹	11 (0,100)	18–59	Not reported	11 (0,100)	18–52	Not reported
MDD ²	15 (0,100)	22–52	Not reported	37 (0,100)	19–55	Not reported
MDD ³	NA	NA	NA	100 (43,57)	20–76	White (100)
Psychosis ¹	NA	NA	NA	77 (72.7,27.3)	16–35	Asian (5.2); Black (46.8) White (42.9) Other (5.2)
Psychosis ²	57 (64.9,35.1)	16–35	Asian (14) Black (8.8) White (71.9) Other (5.3)	121 (61.2,38.8)	16–35	Asian (6.6); Black (38.8) White (50.4) Other (4.1)

MDD¹=Kansas Musical Depression study^{184,185}; MDD²=Russia fMRI Depression Study^{186,187}; MDD³=PDC. Psychosis¹=HCP-EP sample used in the functional coupling loss analyses. Psychosis²=HCP-EP sample used in the gray matter loss analyses. MDD=major depressive disorder. PDC=Perturbation of the Depression Connectome. HCP-EP=Human Connectome Project-Early Psychosis. Other=mixed race/not reported. NA, not available.

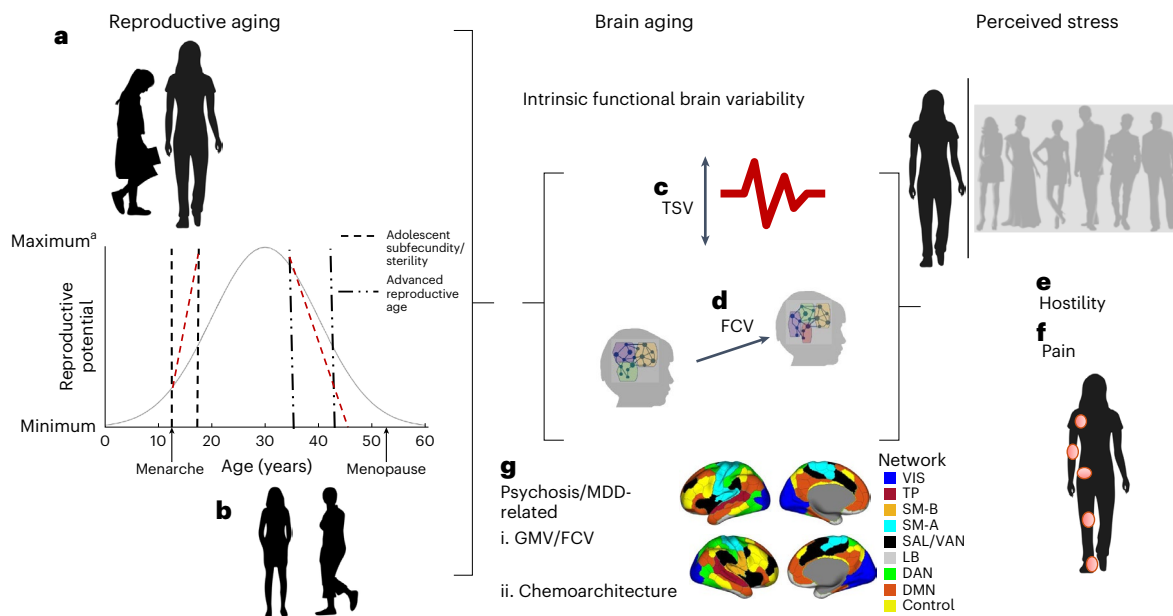


Fig. 1 | Schematic representation of our conceptual model. a–f, Premature reproductive aging in the form of earlier pubertal onset (a) or faster progression towards menopause (b) was hypothesized to be related to patterns of intrinsic variability in time series (TSV) (c) or functional coupling (FCV) (d), suggestive of accelerated maturation/senescence, which would, in turn, predict greater perceptions of hostility (e) and/or pain (f). The dashed red lines in a depict potential trajectories of accelerated reproductive maturation or aging. g, Using the Schaefer brain atlas¹⁶⁵, the spatial profiles of TSV/FCV linking reproductive

aging to stress susceptibility were further examined for their similarity with the atrophy, brain variability and chemoarchitectural fingerprint of disorders typified by accelerated brain maturation/senescence. Schaefer networks: TP, temporo-parietal; SAL-VAN, salience/ventral attention; LB, limbic; DMN, default mode; DAN, dorsal attention; SM-A, somatomotor-A; SM-B, somatomotor-B; VIS, visual. ^aPlot in a and b adapted with permission from ref. 211 under a Creative Commons license CC BY 4.0. Whole-body silhouettes in a, b, e and f are from vecteezy.com.

partly, the modulatory effects of gonadal hormones over four neurotransmitter systems (that is, dopaminergic (DA), serotonergic (5-HT), glutamatergic (GLU) and gamma-aminobutyric acid-related (GABA)) that play a critical role in mental functions relevant to coping with stress (Fig. 1h)^{10,27,63,64}. Importantly, these four neurotransmitter systems are also critically implicated in both psychosis^{65–73} and MDD^{74–80}. Using a multimodal approach, we sought to uncover the neurochemical correlates of the overlap in the reproductive aging and psychosis/MDD-relevant brain maps with the goal of identifying potential targets for future pharmaceutical interventions targeting neuropsychiatric symptoms linked to accelerated reproductive aging. Our conceptual framework is represented schematically in Fig. 1.

Results

The results reported in the following were replicated with the Gordon atlas⁸¹ (Supplementary Information) and their specificity was supported by supplemental tests featuring alternate graph measures sensitive to maturation/aging (Supplementary Fig. 4).

Accelerated reproductive aging is linked to greater FCV

ABCD. The full-sample discovery partial least-squares (PLS) analysis linking Time 1 and Time 2 TSV and FCV, respectively, to aging as well as perceived exposure to pain and interpersonal adversity, identified a sole significant brain-behavior latent variable (LV) pair ($P = 0.017$; shared variance, 37%). Across the ten test folds, the extracted LV pair

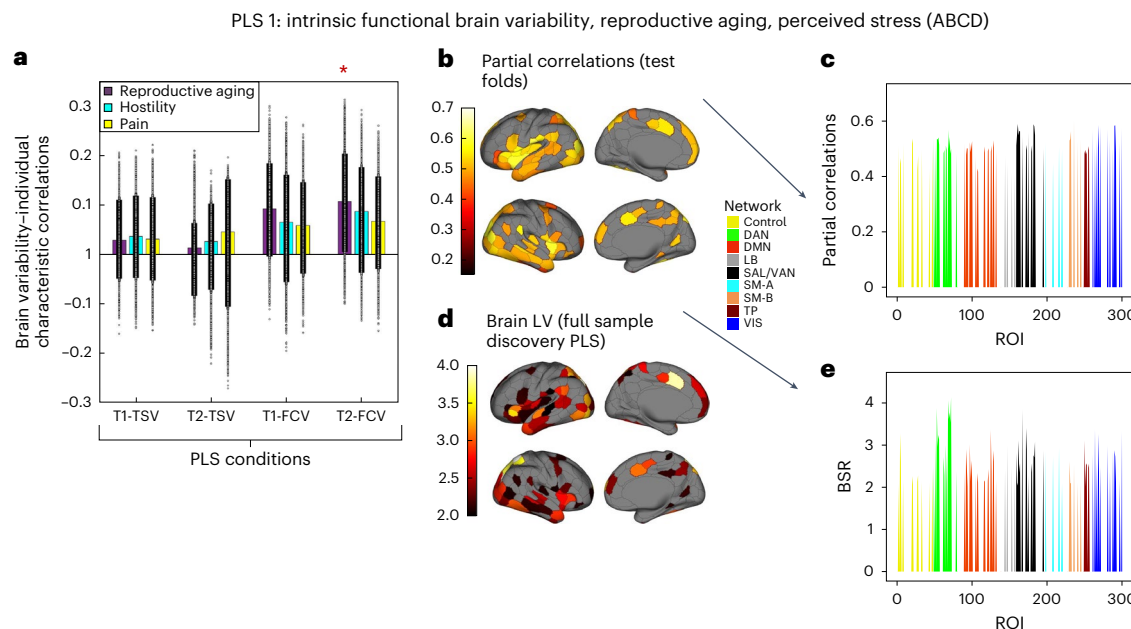


Fig. 2 | The brain LV from the behavioral PLS analysis linking reproductive aging, perceived hostility and pain to TSV and FCV in the ABCD sample.

a, The height of the colored bars indicates the correlation coefficient between the behavioral variables and the predicted brain LV scores (based on a cross-validation procedure) in each condition across all 441 ABCD participants. Error bars, represented as black blocks, constitute the 95% CI values estimated by re-running each correlation on 100,000 bootstrap samples. The individual data points represent the correlation coefficient obtained with each of the 100,000 bootstrap samples. CIs that do not include zero reflect robust correlations between the respective behavioral variable and the predicted brain LV score in a given condition across all participants. The asterisk marks the statistically significant correlation between FCV and accelerated reproductive aging at Time

2 (based on permutation testing as described in the main text). **b**, The Schaefer ROIs that are (1) robustly correlated (based on cross-validated 99% CIs, as described in the main text) with the brain LV in **a** and (2) have an absolute value BSR of at least 2 in the discovery PLS analysis (**d**). These are partial correlations controlling for the confounders listed under ‘Control variables’ in Methods. **d**, The ROIs that have an absolute BSR value of at least 2 and are thus considered to load reliably (at -95% CIs, based on 100,000 bootstrap samples) on the brain LV identified with the discovery PLS analysis in the full sample ($N = 441$). **c,e**, To facilitate interpretation, the Schaefer network-level representations of the ROI-specific results from **b** and **d**, respectively. All bootstrap samples were obtained by sampling with replacement from the original set of 441 ABCD participants. BSR, bootstrap ratio.

was found to reflect the Time 2 link between accelerated reproductive aging and greater FCV ($r = 0.11$, permutation-based $P = 0.029$, 95% confidence interval (CI) = [0.01; 0.20]) (Fig. 2a). This effect was widely expressed and peaked in the visual (VIS), salience/ventral attention (SAL/VAN), dorsal attention (DAN), default mode (DMN) and control systems (Fig. 2b,c) shows the cross-validation and Fig. 2d,e the discovery PLS results).

HCP-A. A similar pair of brain variability-behavior LVs emerged from the full-sample discovery PLS analysis conducted separately in the HCP-A data ($P = 0.046$; shared variance, 34%). As in the ABCD dataset, the extracted LV pair reflected the robust link between accelerated reproductive aging and FCV, a relationship that was cross-validated over all ten test folds, ($r = 0.20$, permutation-based $P = 0.024$, 95% CI = [0.03; 0.35]; Fig. 3a). Thus, greater FCV related to reproductive aging was widespread and most clearly detected in the VIS, DAN, DMN and temporo-parietal (TP) systems (Fig. 3b,d).

FCV mediates the perceived hostility–reproductive aging link
To test whether the sample-specific profiles of FCV mediate the link between accelerated reproductive aging and perceived exposure to pain/interpersonal adversity, we specified the mediational model represented in Fig. 4. Profiles of functional brain variability were estimated separately within each sample as the weighted sum of all region-of-interest (ROI) contributions in the FCV condition. We focused on the FCV condition in the HCP-A data and the Time 2 FCV condition in the ABCD sample, because these were the only conditions in which we observed robust brain–reproductive aging correlations in the ten test folds (Figs. 2a and 3a). The PLS-extracted profiles of FCV mediated the relationship

between reproductive aging and sensitivity to hostility (total standardized indirect effect: 0.014, 95% CI = [0.003; 0.034]), but not pain (total standardized indirect effect: 0.004, 95% CI = [-0.005; 0.017]) (Fig. 4). None of the direct or total effects (reproductive aging–perceived hostility/pain) was statistically significant (all $P > 0.33$), a pattern of results suggestive of an indirect relationship only, which is currently well-accepted in the literature^{82,83}.

Age-related FCV maps, chemoarchitecture and neuropathology

Given the weak association between the confounder-controlled ROI–brain LV correlations estimated in the two samples, separate canonical correlation analyses (CCAs) were conducted for the FCV patterns extracted from the ABCD versus HCP-A data.

In each sample, the discovery CCAs identified a single mode that linked FCV to the chemoarchitecture and disorder-specific neuropathology across all ten test folds (cross-validated r values of 0.50 (ABCD) and 0.66, both $P = 1 \times 10^{-5}$; Fig. 5a,c). The FCV profile associated with accelerated reproductive maturation in the ABCD sample (Figs. 2b and 5b) showed robust positive correlations with the psychosis-, rather than the MDD-relevant FCV and atrophy maps (Fig. 5b,e,f), as well as with areas of higher 5-HT, DA (D1/D2) and GLU receptor density (Fig. 5g–k). Complementarily, the FCV profile related to faster reproductive senescence in HCP-A (Figs. 3b and 5d) was positively associated with the MDD-, rather than the psychosis-relevant FCV and atrophy maps (Fig. 5e,f), but showed robust negative correlations with the 5-HT, DA (D1/D2) and GLU receptor density maps (Fig. 5g–i,k). Put differently, greater FCV linked to faster reproductive aging was observed in areas of lower 5-HT, DA and mGLU5 receptor density.

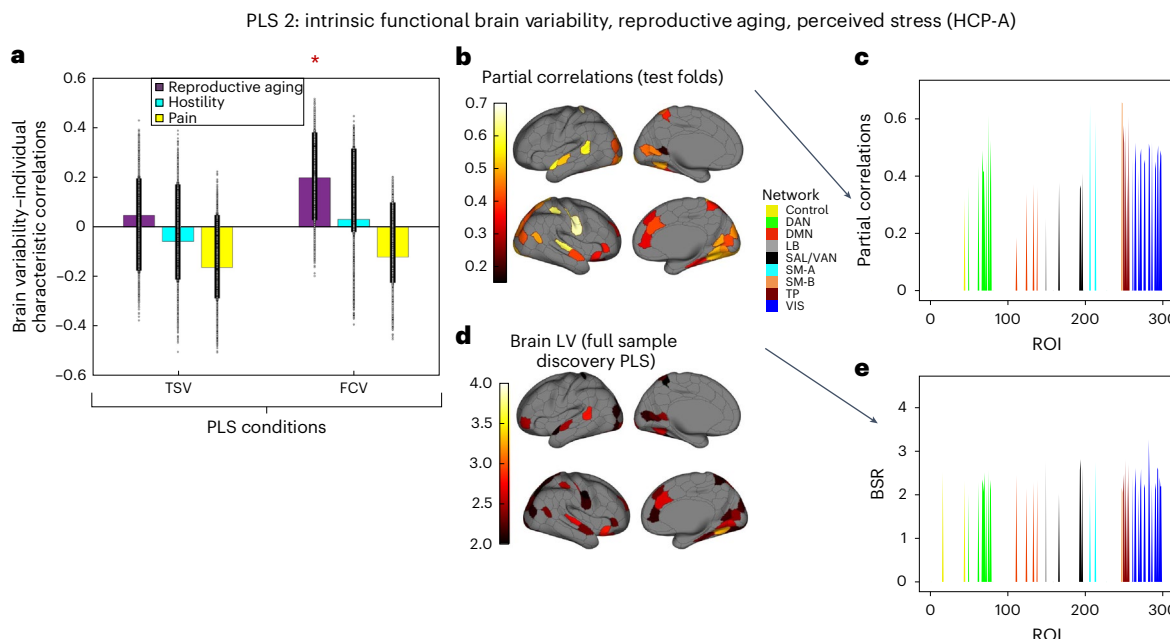


Fig. 3 | The brain LV from the behavioral PLS analysis linking reproductive aging, perceived hostility and pain to TSV and FCV in the HCP-A sample.

a, The height of the colored bars indicates the correlation coefficient between the behavioral variables and the predicted brain LV scores (based on a cross-validation procedure) in each condition across all 130 HCP-A participants. Error bars, represented as black blocks, constitute the 95% CIs estimated by re-running each correlation on 100,000 bootstrap samples. The individual data points represent the correlation coefficient obtained with each of the 100,000 bootstrap samples. The asterisk marks the statistically significant correlation between FCV and accelerated reproductive aging (based on permutation testing as described in the text). CIs that do not include zero reflect robust correlations between the respective behavioral variable and the predicted brain LV score in a

given condition across all participants. **b**, The Schaefer ROIs that are (1) robustly correlated (based on cross-validated 99% CIs, as described in the main text) with the brain LV in **a** and (2) have an absolute value BSR of at least 2 in the discovery PLS analysis (**d**). These are partial correlations controlling for the confounders listed under ‘Control variables’ in Methods. **d**, The ROIs that have an absolute BSR value of at least 2 and are thus considered to load reliably (at ~95% CIs, based on 100,000 bootstrap samples) on the brain LV identified with the discovery PLS analysis in the full sample ($N = 130$). **c,e**, To facilitate interpretation, the Schaefer network-level representations of the ROI-specific results from **b** and **d**, respectively. All bootstrap samples were obtained by sampling with replacement from the original set of 130 HCP-A participants.

Control analyses. A series of partial correlation analyses investigated whether the PLS-extracted age group FCV LV (Supplementary Fig. 7a,b,d,e), the ROI-specific intrinsic functional coupling (FC), estimated separately within each sample (Supplementary Fig. 8), and the complementary reproductive aging brain LV (that is, the ABCD brain LV for the HCP-A sample; the HCP-A brain LV for the ABCD sample) would impact the identified CCA modes (Fig. 5a,c and Supplementary Fig. 6a,c) or the structure of the corresponding cross-validated canonical loadings (Fig. 5b,d). With the exception of the neuropathology GMV variable in the ABCD sample, these additional controls did not impact any of the CCA results reported above (partial r values for the cross-validated CCA modes from 0.38 to 0.44, all $\text{spin test } P = 1 \times 10^{-5}$; Supplementary Fig. 9).

Discussion

Although independently associated with stress exposure/reactivity^{36,37} and earlier reproductive maturation^{28,39}, the role of neurodevelopment in explaining the link between the two has been challenging to prove. Our investigation (see Fig. 6 for STROBE flowchart) takes a first step towards addressing this issue by demonstrating that the relationship between faster reproductive aging and perceptions of greater interpersonal adversity is mediated by patterns of intrinsic variability in functional brain organization (that is, FCV), spanning slower to faster intrinsic timescale networks^{84,85}. The identified FCV patterns showed age-group specificity with regard to spatial extent and composition, as well as developmental significance. In adolescence, these FCV patterns were widely expressed and suggestive of delayed brain development relative to same-chronological-age peers^{52,53}, results that resonate with recent evidence linking a younger estimated brain age to greater psychiatric symptom burden in the transition from childhood to young

adulthood⁸⁶. Of note, a robust relationship between accelerated reproductive maturation and greater FCV emerged only at Time 2, plausibly because the corresponding trending association observed at Time 1 was partly obscured by the functional brain network ‘immaturity’ (that is, higher FCV) of the entire ABCD sample at this earlier assessment. In middle adulthood, the FCV patterns linking earlier reproductive senescence and perceptions of greater interpersonal adversity implied steeper brain aging^{48,50,54} and were observed primarily in the VIS, DMN and attentional networks, all of which are particularly vulnerable to aging-related functional dedifferentiation processes^{50,87}. Importantly, we only found evidence of a robust indirect positive relationship between reproductive maturation/senescence and perceived hostility, suggesting that it is the emergence of the age-group-specific FCV profiles that may underpin the bidirectional link between aging and social stress sensitivity^{1,10}.

The involvement of somatomotor (SM) areas in the maturational and aging brain profiles dovetails with evidence on its role in tracking dynamic whole-brain state transitions⁸⁸ and its contribution to the stability of FC patterns⁵⁴. In line with the documented relevance of neuronal hyper-excitability and intrinsic FC, broadly, as well as SM FC, specifically, to MDD^{89–92} and psychosis^{69,72,93,94}, we report a robust, yet age-specific, association between the identified FCV patterns and normative profiles of FCV and GMV loss in MDD and psychosis, respectively. In adolescence, the FCV patterns mediating the link between reproductive maturation and perceived interpersonal adversity showed a positive correlation with the FCV map tracking psychosis, rather than MDD, symptom severity, as well as the associated GMV loss map. Thus, slower functional brain development^{52,53} may represent one mechanism through which accelerated reproductive maturation and

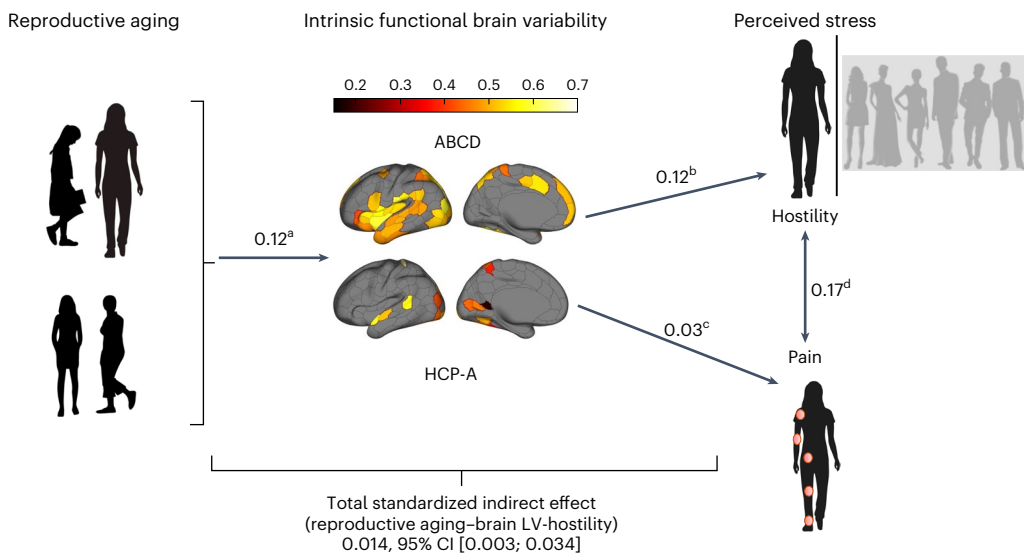


Fig. 4 | Mediational model linking reproductive aging to perceived hostility and pain via variability in functional brain organization across the ABCD and HCP-A samples. The PLS-extracted profiles of FCV mediated the relationship

between reproductive aging and sensitivity to hostility, but not pain. ^a $P = 0.004$. ^b $P = 0.008$. ^c $P = 0.41$. ^d $P = 0.0001$. All P values are two-tailed. Whole-body silhouettes are from vecteezy.com.

perceived interpersonal adversity increase vulnerability to psychosis, a disorder related to faster structural, but not functional brain aging^{58,62}. While delayed emergence of cognitive control skills, and thus poorer stress-coping resources^{95,96}, arise as primary candidates for explaining the psychological implications of the above inter-relationships, more-in-depth studies on the associations between reproductive aging, perceived hostility and neurodevelopment are warranted.

In contrast, the middle-aged FCV profile mediating the relationship between earlier reproductive senescence and perceived hostility overlapped areas of normative MDD-related GMV and regions showing FCV patterns that tracked MDD symptom severity. Dovetailing with evidence on the relevance of SM, VIS and attentional networks to the pathophysiology of MDD^{91,92}, our results imply that accelerated aging of the aforementioned systems constitutes one mechanism through which earlier reproductive senescence and interpersonal adversity may heighten risk for MDD in later life. This interpretation is consistent with extant theory and evidence linking neurocognitive aging to a declining ability to engage strategically with the external environment in the here and now and thus a likely poorer capacity to cope effectively with novel challenges in the external milieu^{97,98}.

The more robust molecular correlates emerged for the adolescent FCV profile and spanned several neurotransmitter systems modulated by gonadal hormones and implicated in functional network dynamics, stress reactivity and psychosis-related pathophysiology^{10,69,73,99,100}. Echoing earlier studies on the modulatory effect of estradiol on dopaminergic systems^{64,101}, the FCV patterns associated with earlier reproductive maturation overlapped with areas rich in D2 and, to a lesser extent, D1 receptor density. These effects are consonant with the well-documented relevance of D1/D2 receptors to stress susceptibility¹⁰², psychosis pathology (D2 (ref. 73)) and their differential involvement in maintaining (D1) versus updating (D2) mental representations in the service of adjustment to environmental challenges^{103,104}. The overlap between the FCV profile related to faster reproductive maturation and regions of higher GLU receptor density fits nicely with the putative role of excitation/inhibition imbalance in psychosis^{68,72} and the involvement of mGLUS in responses to social stress³⁴. Broadly, the chemoarchitectural findings underscore the potential wide-ranging impact of earlier progression towards a key female hormonal transition. They thus dovetail nicely with epidemiological evidence that adolescence is a key period for the emergence of multiple psychiatric disorders⁶¹.

This interpretation fits well with the corresponding neuropathological results, because risk for psychosis relates to multiple neuropsychiatric comorbidities⁵⁷.

More generally, if accelerated reproductive maturation or senescence is experienced as an internal stressor (for example, an inner alarm clock signaling the potential for an earlier demise¹⁹), then our findings could speak to extant stress-related theories¹⁰⁵. The FCV patterns linking faster reproductive aging to greater perceived hostility could reflect an adaptation to chronic stress¹⁰⁶ through which an internal stressor is projected onto the external social environment to alleviate its threat value (that is, the negative affective experience stemming from perceptions of faster reproductive maturation/aging is misattributed to perceptions of greater interpersonal adversity). Alternatively, the observed FCV patterns could reflect a sensitizing mechanism that drives reciprocal interactions between internal and external stressors (that is, perceptions of accelerated reproductive maturation/aging increase vigilance to signs of interpersonal adversity and vice versa). Targeted interventions that address perceptions of biological aging, their associated interpretations (with regards to long-term survival) and perceptions of social support availability may help mitigate these effects.

To disentangle the functional significance of the FCV patterns associated with accelerated reproductive maturation/senescence from the significance of those linked to typical age-group differences, we compared the ABCD and HCP-A samples (Supplementary Fig. 7). These analyses revealed that FCV patterns typical of middle adulthood (rather than adolescence) correlate positively with the FCV and GMV maps tracking psychosis (rather than MDD) severity (Supplementary Fig. 7c,f). Thus, in line with epidemiological evidence of higher MDD prevalence in adolescence and of longitudinal increases in MDD adolescent cases^{10,107}, our results suggest that, for typically developing female individuals, early teenage years may be linked to greater vulnerability to MDD, rather than psychosis spectrum disorders. Complementarily, our results suggest that typical middle-aged women may be more likely to develop psychosis spectrum disorders (rather than MDD). This effect could stem from age-related vulnerability to attentional problems (Supplementary Fig. 10a,b), which, in turn, increases risk for multiple psychiatric and neurological disorders with which psychosis shares a substantial number of brain pathways¹⁰⁸. This conjecture is compatible with the observed chemoarchitectural

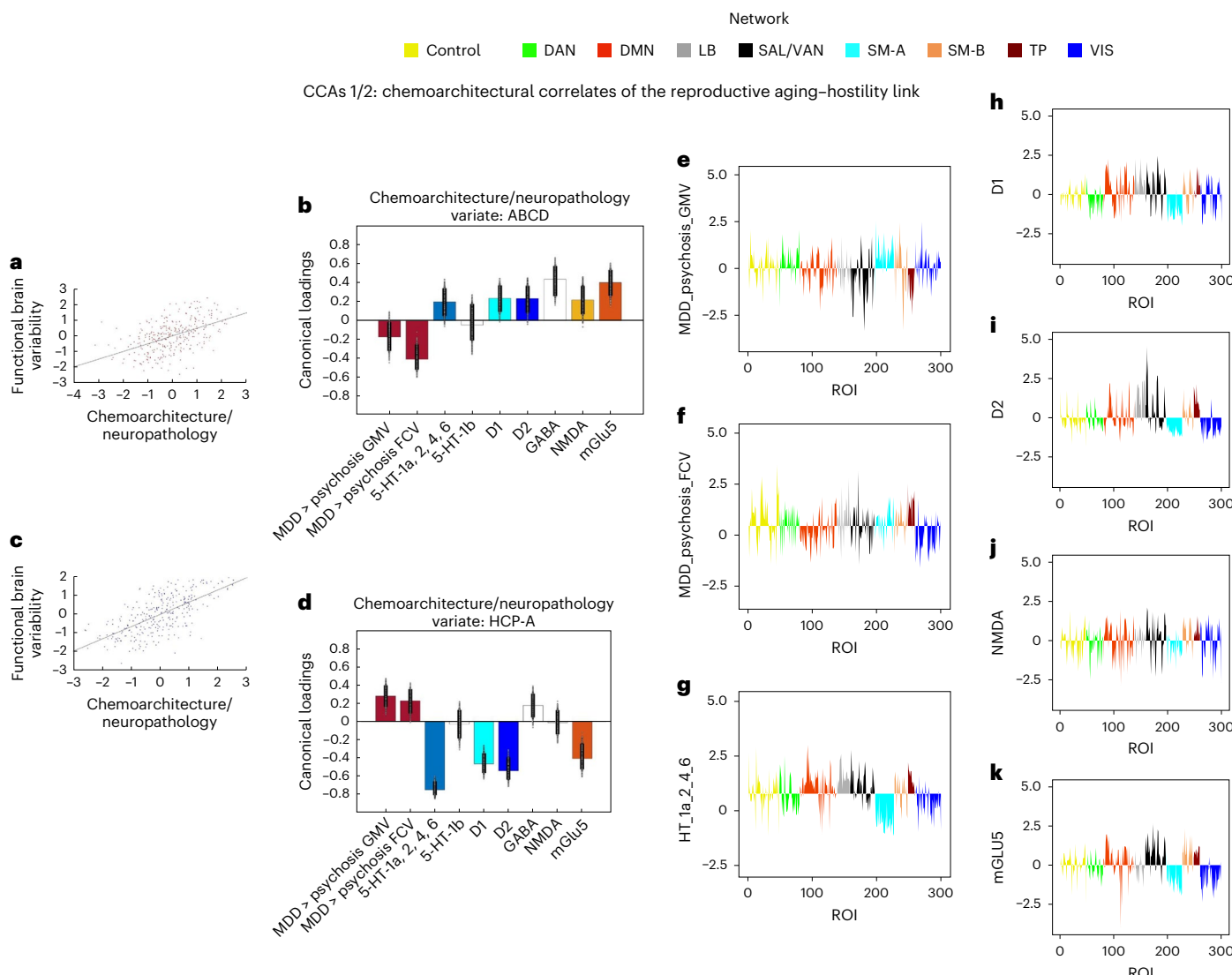


Fig. 5 | Chemoarchitectural correlates of the reproductive aging–hostility link. Disorder-specific GMV loss/FCV and receptor density maps linked by CCA to the brain variability profiles observed in the ABCD and HCP-A samples, respectively (cf. Figs. 2 and 3). **a,c**, Scatter plots describing the linear relationship between predicted values of the brain and the disorder-specific GMV loss/FCV/receptor density CCA variates across the 300 ROIs from the Schaefer atlas for the ABCD (**a**) and HCP-A (**c**) samples. **b,d**, Correlations between the observed disorder-specific/receptor density maps and the predicted value of their corresponding canonical variate across all test CCAs for the ABCD (**b**) and HCP-A (**d**) samples. Error bars,

represented as black blocks, constitute the 99% CIs estimated by re-running each correlation on 100,000 bootstrap samples. The individual data points represent the correlation coefficient obtained with each of the 100,000 bootstrap samples. Colored columns correspond to variables with robust loadings on their variate in both the Schaefer and Gordon atlas data (based on the bootstrapping-derived 99% CIs). The bootstrap samples were obtained by sampling with replacement from the 300 Schaefer ROIs. **e–k**, MDD/psychosis difference GMV loss (**e**) and FCV (**f**) maps, as well as the 5-HT (**g**), D1 (**h**), D2 (**i**), NMDA (**j**) and GluR5 (**k**) receptor density maps. NMDA, *N*-methyl-D-aspartate.

map correlated with age-group differences in FCV, which spanned neurotransmitter systems relevant to cognitive control and responses to stress (GABA^{109,110}), memory persistence and flexibility^{103,111}, learning (NMDA¹¹²) and broader psychiatric vulnerability and (un)successful aging (5-HT^{113,114}) (Supplementary Fig. 7c,f).

Limitations and future directions

Our investigation has several limitations that pave the way for future research venues. First, its primary cross-sectional design precludes any conclusions regarding the causality of the reported effects, a caveat that needs to be addressed in carefully controlled longitudinal investigations and/or cross-species experimental manipulations.

Second, due to data availability, our study drew on predominantly Caucasian samples. The neuropathological fingerprint of common psychiatric disorders shows some variability with ancestry, comorbidity with

medical conditions and/or country-level socioeconomic conditions¹¹⁵. Consequently, future studies with larger and more diverse samples could elucidate the boundary conditions of the effects reported here.

Third, our study focused on the adverse outcomes of accelerated reproductive senescence^{116–118}. Nonetheless, certain (epigenetic) aging patterns (that is, DNA methylation at certain promoter regions) can have a neuroprotective effect¹¹⁹. Characterizing these aging patterns and their susceptibility to environmental modulation, including perinatal factors (for example, maternal depression¹²⁰) would be worth pursuing in the future.

Fourth, our research probed the relevance of variability in resting-state functional brain dynamics. However, cognitive traits, including those implicated in stress responses, show context-specific associations with brain dynamics¹²¹. Hence, use of a variety of task paradigms (for example, naturalistic movie viewing¹²², acute stress manipulations)

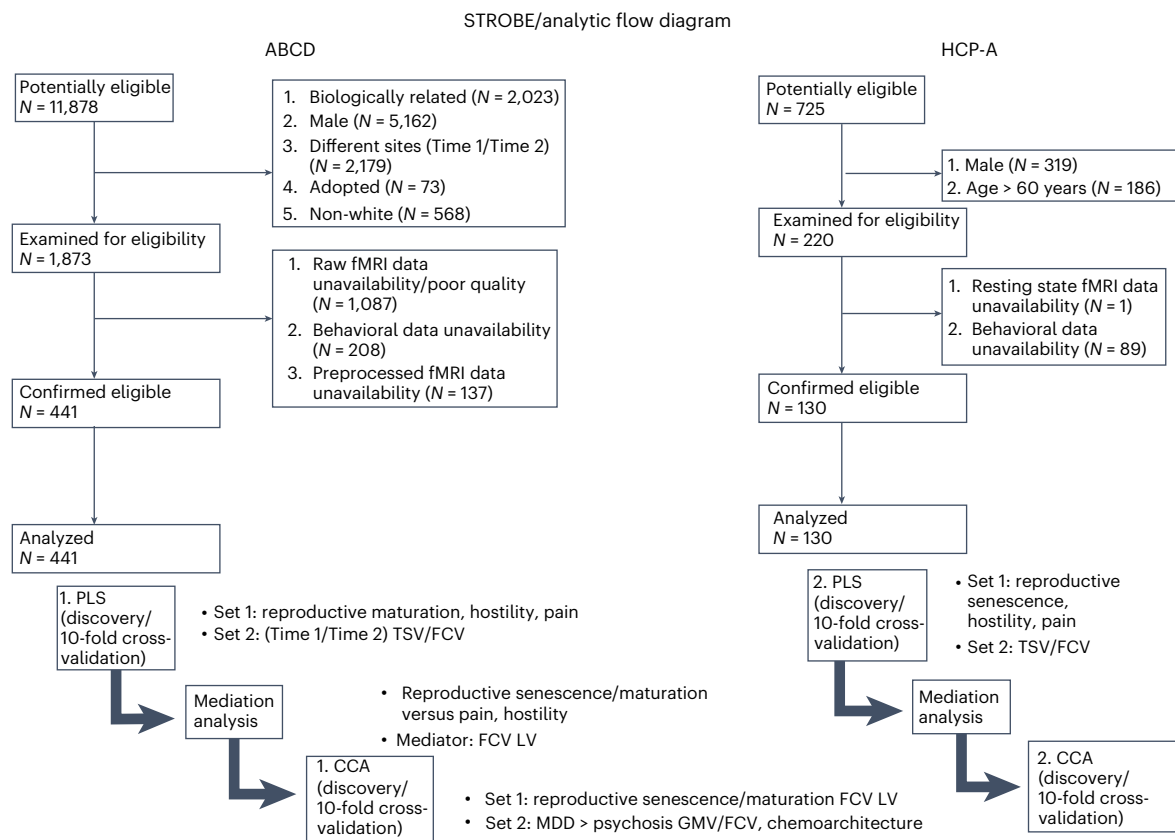


Fig. 6 | STROBE flowchart describing sample selection and outlining the main analytic steps. The ABCD and HCP-A data were downloaded as part of a package with the data reported in ref. 166 and ref. 155, respectively. The rationale for doing

so was twofold: (1) allow cross-study comparisons and (2) include participants who provided good quality data across multiple contexts (in particular, for ABCD, given the age of the sample).

and multiple neural dynamics indices^{123,124} could enhance the applicability of the present results and shed light on the specific mechanisms linking accelerated senescence to pain versus hostility sensitivity (cf. refs. 32,125).

Fifth, we failed to find an association between TSV and either accelerated reproductive aging or perceived stress. Associations between resting-state TSV and cognitive performance or stress exposure have been documented in older samples, both from the earlier and later life stages^{43,51}. Alternatively or additionally, the link between TSV and stress-relevant variables may be most likely to emerge in paradigms assessing blood-oxygen-level-dependent (BOLD) signal dynamics on externally oriented attentional tasks, because higher TSV has been shown to foster finer-grained perceptual processing⁴⁴. Therefore, future investigations including more age-varied samples and assessing TSV during both rest and externally oriented processing tasks could characterize its relevance to accelerated aging and stress susceptibility.

Sixth, our investigation focused on relatively stable patterns of neurobiological aging. However, perceived exposure and susceptibility to stressors is also modulated by reversible brain-aging factors (for example, sleep deprivation^{126,127}), whose short-versus long-term impact on brain-network organization and dynamics is worth exploring.

Seventh, because biological aging is a multimodal process, use of multiple indicators beyond reproductive senescence¹²⁸ could further elucidate shared mechanisms underpinning stress susceptibility, connectomic maturation/senescence and cognitive functioning at different life phases (cf. ref. 129). This research could also pinpoint indicator-specific sequelae, such as those linked to the accumulation of senescent cells and subsequent chronic neuroinflammation, mediated by microglial and astroglial activation, which hinders synaptic

plasticity and brain-network functioning¹³⁰. Use of multiple aging indicators, including those indexing neuroinflammation, would further facilitate investigations into the sex specificity of the associations among biological senescence, dynamic connectomics and stress vulnerability. Such studies would build on extensive evidence of sex differences in brain-immune system interactions^{131,132}, brain network organization¹³³, genetically modulated risk for stress-related disorders^{134,135} and responses to pain/hostility^{7,136-138}.

Eighth, although we focused on two key female hormonal transitions, mounting evidence attests to the long-term neurobiological impact of an additional pivotal hormonal event, specifically, pregnancy and motherhood¹³⁹. For instance, pregnancy is linked to changes in intrinsic functional network organization, reduced brain inflammation and increased neurogenesis^{140,141}, which, in the long term, may foreshadow a younger brain age and foster higher cognitive reserve^{139,142}. Most relevant to the present study is the finding of post-pregnancy changes in the relationship between cycling hormones and psychological stress responses, which probably reflects alterations of GABA-ergic signaling and HPA-axis output¹⁴³. Hence, pregnancy may impact the inter-relationships among reproductive aging, perceived stress and intrinsic FCV, a possibility worth exploring in future research.

Finally, FCV did not mediate the reproductive aging–pain relationship. However, pain is multifaceted and best viewed through a biopsychosocial lens¹⁴⁴, as its physical features (for example, location—single site versus multi-region) interact with psychological and sociocultural factors to shape experience¹⁴⁵. Given the high prevalence of chronic pain in both adolescent¹⁴⁶ and middle-aged¹⁴ samples, more fine-grained assessments of pain, including location and duration of each episode, could advance understanding of its relevance to neurobiological aging and stress susceptibility¹⁴⁷.

Conclusions

Using cross-sectional data primarily, we have documented age-specific profiles of variability in functional brain organization that mediate the relationship between accelerated reproductive aging and perceptions of interpersonal adversity in adolescence and middle age. The two profiles indicated divergent changes in aging-related trajectories (that is, delayed in adolescence, but accelerated in middle adulthood) and showed opposite relationships with patterns of functional neural network variability and cortical atrophy observed in psychosis versus MDD. Our findings speak to the importance of brain dynamics in mediating the relationship between reproductive senescence and perceived stress, while also underscoring its age-specific role in alleviating versus enhancing risk for psychological maladjustment.

Methods

Participants

Both samples contributed complete data on all the analyzed variables (one time point for the HCP-A sample; baseline/Time 1 and two-year follow-up/Time 2 data for the ABCD sample). Inclusion of the imaging data was guided by recommendations of the ABCD and HCP-A teams, respectively. Because pubertal timing, including its association with mental versus cardiometabolic health and, to a lesser extent, menopausal onset, vary with racial background^{148–151}, and there were insufficient participants to allow well-powered analyses of racial differences, the samples were exclusively (ABCD) white—as reported by the children’s parents—or predominantly (62%, HCP-A) white, as self-reported by the participants. This choice is justified, as one of the comparison clinical groups (that is, MDD) with relevant data was also exclusively white. Participants in both samples were biologically unrelated to one another (that is, they did not share a family ID). Table 1 summarizes the demographic information for both the ABCD and HCP-A samples. The demographic information for the MDD and psychosis samples is included in Table 2. Figure 6 contains the STROBE flow diagram detailing participant selection for our present study.

ABCD. The present research uses baseline and two-year follow-up data downloaded in November 2021 as part of the ABCD Study Curated Annual Release 4.0 (<https://data-archive.nimh.nih.gov/abcd>). The non-imaging variables were screened for completeness. Inclusion of the imaging data was guided by recommendations of the ABCD team. Specifically, global information about the data recommended for inclusion by the ABCD team was recorded as a binary decision (0 ('no')/1 ('yes')) in the 'abcd_imgincl01' file, which was part of Annual Release 4.0. Run-specific information was recorded as 'fail/pass/unspecified/no value' under 'qc_outcome' in the file 'fmriresults01'. We only used data from participants who had passed the qc for six resting-state runs (three runs at baseline and two-year follow-up, respectively).

All participating parents provided informed consent, and the participating children provided assent in accordance with the guidelines of the local research ethics review boards across the 21 participating sites (that is, Children’s Hospital Los Angeles, Florida International University, Laureate Institute for Brain Research, Medical University of South Carolina, Oregon Health & Science University, SRI International, University of California San Diego, University of California Los Angeles, University of Colorado Boulder, University of Florida, University of Maryland at Baltimore, University of Michigan, University of Minnesota, University of Pittsburgh, University of Rochester, University of Utah, University of Vermont, University of Wisconsin-Milwaukee, Virginia Commonwealth University, Washington University in St Louis and Yale University). Participants were compensated for time and travel expenses. More specific compensation details have not been publicly released.

HCP-A. Participants were aged 36 to 60 years, an interval that captures the transition from reproductive to late post-menopausal status. Exclusion criteria included sensory (hearing/vision) deficits, uncontrolled

high blood pressure, major organ failure and a Montreal Cognitive Assessment (MoCA) score of 19 or lower¹⁵².

All participants provided informed consent in accordance with the guidelines of the local research ethics review boards across the four participating sites (that is, University of California Los Angeles Medical School, University of Massachusetts Medical School, University of Minnesota Medical School and Washington University at St Louis). Participants were compensated for time and travel expenses up to US\$400. More specific compensation details have not been publicly released.

Reproductive aging

ABCD. Reproductive aging was assessed with the five-item Pubertal Development Scale (PDS), which is significantly correlated with other indices of pubertal development, including physician ratings¹⁵³. The questionnaire comprises three gender-general items (growth spurt, changes in skin and hair growth) and two gender-specific items (breast development and menarche (girls)). The instrument, which uses a four-point Likert-type response format, ranging from 1 (no development) to 4 (development already completed), was completed separately by the youth and their guardian/parent. Because youth ratings showed poorer reliability at baseline (Cronbach’s alpha of 0.54), we opted to use parental ratings at both baseline and two-year follow-up (Cronbach’s alpha of 0.65 and 0.78 at baseline and two-year follow-up, respectively). For participants with available hormonal data, we verified that parental PDS ratings showed the expected positive correlation with pubertal hormones, both at baseline— $r(423) = 0.27, P < 0.001$ (testosterone), $r(414) = 0.28, P < 0.001$ (dehydroepiandrosterone (DHEA)), $r(409) = 0.09, P = 0.06$ (estradiol)—and at the two-year follow-up— $r(317) = 0.25, P < 0.001$ (testosterone), $r(313) = 0.29, P < 0.001$ (DHEA), $r(299) = 0.17, P = 0.003$ (estradiol).

An index of accelerated maturation relative to same-chronological-age peers was computed at each time point by regressing from the PDS score the youth’s chronological age, such that a positive residual score indicated accelerated reproductive aging^{1,29} (Supplementary Fig. 1a presents the distribution of accelerated maturation scores across the ABCD sample). This residual score showed robust positive associations with contemporaneous levels of DHEA and testosterone across both time points, (r values from 0.22 to 0.28, all $P < 0.001$). However, a significant relationship between accelerated reproductive maturation and estradiol levels emerged only at the two-year follow-up ($r(299) = 0.17, P = 0.003$).

HCP-A. Responses on the self-report survey of the Stages of Reproductive Aging Workshop (STRAW-10¹⁵⁴) were used to estimate menopausal status. We used the same strategy as in ref. 155 to convert STRAW codes to menopausal status. In the 110 participants with available data, more advanced menopausal status correlated with higher levels of follicle stimulating hormone ($r(107) = 0.81, P < 0.001$) and lower levels of estradiol ($r(107) = -0.41, P < 0.001$) after controlling for whether blood was collected after fasting¹⁴⁹.

Reproductive aging was estimated by regressing out chronological age from the menopausal status index described above. Positive residual scores reflected accelerated reproductive aging, and negative scores decelerated reproductive aging (Supplementary Fig. 1b presents the distribution of accelerated aging scores across the HCP-A sample). As expected, this residual score correlated positively with follicle stimulating hormone levels ($r(107) = 0.32, P < 0.001$), but not estradiol levels ($r(107) = -0.05, P > 0.60$), potentially because the latter is more strongly modulated by chronological age-related processes relevant to menopause. Finally, we verified that age at menarche, a significant predictor of age at menopause, was not significantly associated with this index of reproductive aging ($r(128) = -0.08, P = 0.34$).

Perceived stress

None of the perceived stress measures described below had a cutoff for severe or clinically significant pain experience or perceived hostility

because they were all primarily intended to assess individual differences in healthy individuals. Two-independent-samples Mann–Whitney U-tests confirmed that the distribution of neither experienced pain (standardized test statistic 0.27, $P = 0.79$) or perceived hostility (standardized test statistic 0.46, $P = 0.64$) is statistically different in the ABCD versus HCP-A samples (details on the measures are presented in the following).

Pain experience

ABCD. The two-year follow-up was the earliest time point at which participants' exposure to pain in the month preceding their study participation was assessed with four items from an adjusted version of the Seattle Child And Adolescent Pain questionnaire¹⁵⁶, which gauged presence/absence of pain (0/1), highest pain intensity (10-point Likert-type scale from '1 not at all' to '10 the worst'), typical duration of a painful episode (four-point Likert-type scale from '1 less than an hour' to '10 all day') and the extent to which pain hindered engagement in typical activities (10-point Likert-type scale from '1 not at all' to '10 stopped me from doing anything'). This revised four-item scale showed good reliability (Cronbach's alpha of 0.78). Based on the observed scores (Supplementary Fig. 1), ~50 participants reported having experienced some pain during the month preceding their study participation, with most pain episodes being rated as moderate to severe (Supplementary Fig. 1c), although relatively short (Supplementary Fig. 1d) and with reduced impact on daily activities (Supplementary Fig. 1e).

HCP-A. Participants' exposure to pain during the preceding week was quantified through their responses to two National Institutes of Health (NIH) Toolbox measures: the one-item Pain Intensity Survey ('1 no pain' to '10 worst pain imaginable') and one item from the Pain Interference Survey, which assesses the extent to which pain interfered with daily activities ('1 not at all' to '5 very much'). Data unavailability prohibited use of other, domain-specific items from the Pain Interference Survey. However, we think that for the sake of comparability with the ABCD measures, use of the above two items is best advised. Score on the two pain items were strongly correlated (r of 0.74), which is why they were first standardized across participants and then averaged to create a single index of pain exposure/sensitivity. Based on the observed scores, approximately half the sample reported some pain in the week preceding their participation (Supplementary Fig. 1f), which had some impact on their daily activities (Supplementary Fig. 1g).

Perceived hostility

ABCD. At the two-year follow-up, participants completed the 18-item Revised Peer Experiences Questionnaire¹⁵⁷. This measure uses a five-point Likert-type scale ('1 Never' to '5 A few times a week') to gauge the extent to which the respondent had been victimized in the past (for example, 'Another kid gossiped about me so others would not like me'). The nine victimization-relevant items showed good reliability (Cronbach's alpha of 0.80) and were averaged to create an index of perceived hostility/interpersonal adversity. Although the perceived hostility scores were relatively low (Supplementary Fig. 1h), ~75% reported having experienced some form of victimization in the past.

HCP-A. The eight-item Perceived Hostility Survey from the NIH Toolbox gauged participants' perceptions of having been treated poorly by people in their lives in the month preceding their study participation. The measure uses a five-point Likert-type scale ('1 Never' to '5 Always') to assess the frequency with which others have criticized, yelled, argued with the participant. The scale showed good reliability (Cronbach's alpha of 0.91) and the responses to the eight items were averaged to create an index of perceived hostility. Inspection of Supplementary Fig. 1i revealed that 88% of the participants had experienced some interpersonal adversity in the month preceding their study visit.

Functional brain variability

These analyses focused on regional TSV and cross-regional time-series variability (that is, FCV), because these measures are widely used to capture distinct aspects of functional MRI (fMRI) dynamics¹⁵⁸. TSV captures variability in the BOLD signal within an individual brain region, which is thought to reflect that region's capacity to adjust its activity in response to changes in the external milieu and, thus, represent environmental dynamics more accurately¹⁵⁹. FCV captures variability in pairwise regional BOLD signal correlations and, as such, it is regarded as a marker of (in)stability in functional brain network organization⁴⁸. We selected dynamic, rather than static, functional indices because of their relevance to environmental adjustment, including psychopathology, and sensitivity to broader biological aging processes^{47,48,159,160}. Specifically, past research has shown that, in adulthood, greater TSV predicts superior cognitive performance and treatment outcome in individuals with social anxiety disorder, whereas greater FCV has been linked to higher anxiety and accelerated metabolic aging. Our focus on regional rather than whole-brain measures provides the spatial specificity required for investigating associations with receptor and neuropathological maps.

Resting-state scans. Both samples contributed four resting-state fMRI (rfMRI) scans (eyes open with passive crosshair viewing) for a total of 20 (ABCD) or 26 (HCP-A) minutes at each sampled time point (ABCD, baseline and two-year follow-up; HCP, one time point). For the ABCD sample, due to data availability, we used only three scans from each time point (six resting-state scans in total). In the HCP-A sample, two rfMRI scans were acquired with an anterior-to-posterior (AP) phase encoding sequence and the other two with a posterior-to-anterior (PA) phase encoding sequence. Because comparisons with the ABCD data were based on a single time point, we used only two of the four rfMRI scans so as to make the scan duration comparable across samples. To facilitate potential future comparisons with the HCP-A task fMRI data on inhibitory control, which were collected with a PA phase encoding sequence, we only used the two resting scans acquired with a PA phase encoding sequence.

MRI data acquisition

The ABCD participants were scanned across 21 US sites, with a protocol harmonized for Siemens Prisma, Philips and GE 3T scanners, whereas scanning for the HCP-A sample was performed across four US sites on Siemens Prisma 3T scanners (32-channel coil). For both samples, to account for magnet and sociodemographic differences among sites, we introduced site ID as a covariate in all analyses. A similar multiband acquisition sequence was used for both samples (see refs. 161,162).

fMRI data preprocessing

ABCD. Our analyses used minimally preprocessed rfMRI data (described above), which was available as part of the ABCD Study Curated Annual Release 4.0. All 441 participants contributed three complete resting-state runs at baseline/Time 1 and the two-year follow-up/Time 2, for a total of six resting-state scans across the two time points (see the 'Participants' section for the quality-control checks used in this study).

The main processing steps applied to these data by the ABCD Study team are outlined as follows (for further details on specific steps, see ref. 162). The minimal preprocessing pipeline applied to the rfMRI data involved correction for head motion, spatial and gradient distortions, bias field removal and co-registration of the functional images to the participant's T1-weighted structural image. We further applied the following steps: (1) elimination of initial volumes (eight volumes (Siemens, Philips), five volumes (GE DV25) and 16 volumes (GE DV26)) to allow the MR signal to reach steady-state equilibrium, (2) linear regression-based removal of the mean time courses of cerebral white matter (WM), gray matter (GM) and cerebrospinal fluid (CSF), as well

as the quadratic trends and 24 motion terms (that is, the six motion parameters, their first derivatives, and squares from the time course of each Schaefer parcel). Before being regressed, the motion terms were filtered to eliminate signals within the respiratory effect range (that is, 0.31–0.43 Hz, cf. ref. 163).

HCP-A. The rfMRI data were processed by applying the Generic fMRI Volume and Surface Processing Pipelines, multi-run independent component analysis (ICA) FIX denoising and multimodal surface-matching registration, as detailed in ref. 164.

ROI definition

Our main fMRI analyses featured the Schaefer 300 parcel-functional atlas¹⁶⁵, downloaded from <https://github.com/ThomasYeoLab/CBIG>. We used the 17 functional network version of the atlas, which is available in the Montreal Neurological Institute (MNI) standard space.

ABCD. As in refs. 166,167, to align the atlas with the participants' native space for each resting-state run, the following steps were implemented in Functional Magnetic Resonance Imaging of the Brain Software Library (FSL): (1) the middle image in each resting-state run was converted to MNI space (via the MNI-152 brain template available in FSL), and the inverse transformation (MNI-to-participant native space) was estimated; (2) the inverse transformation was used to align the Schaefer atlas to each participant's functional images, separately for each resting-state run, based on nearest-neighbor interpolation (to keep the integer values of the ROI IDs).

HCP-A. Voxel-wise time series were extracted and averaged within each of the Schaefer ROIs using the 'cifti-parcellate' command with the MEAN method in the Connectome Workbench (<https://www.humanconnectome.org/software/get-connectome-workbench>).

TSV

Within each element of fully preprocessed resting-state run data, ROI-level TSV was computed as the within-individual standard deviation (s.d.) of BOLD signal fluctuations over time⁴⁴. This is the simplest measure of variance-based neural variability¹⁵⁹, which has been robustly implicated in lifespan development⁴³ (for a review of relevant findings, see ref. 159) and psychopathology^{160,168}. Importantly, this s.d.-based measure of neural variability is strongly correlated with an alternative deviance-based index of TSV based on mean-squared differences between successive time series^{169,170}, particularly in datasets (such as the present ones) where preprocessing included the removal of linear and quadratic trends in the BOLD signal.

ROI-to-ROI correlations

Each resting-state run was broken down into 24-s-long (that is, 30 volumes) non-overlapping windows for a total of 33 windows at each time point in the ABCD sample and 30 windows in the HCP-A sample. The window length and type (that is, non-overlapping) were selected with the goal of augmenting sensitivity to patterns of dynamic functional brain reconfiguration and individual differences in such processes. Sliding windows that were -30 s long met both criteria^{171–173}.

Pairwise Pearson correlations between regional time series extracted from the Schaefer-atlas ROIs were computed separately in MATLAB and expressed as Fisher's z-transformed scores. As per previous work¹⁷⁴, we retained the positive Fisher's z-scores and set negative values to zero.

Network-level analyses

The Network Community Toolbox (NCT)¹⁷⁵ was used to estimate all network-level metrics.

To characterize patterns of ROI-based clustering in functional community organization during awake rest, we used a multilayer

generalized Louvain-like community detection algorithm¹⁷⁶ and implemented it in the NCT^{155,166}. As in earlier works^{155,166,174,177}, the two free parameters in the modularity quality optimization were set to the default value of 1 (the spatial resolution parameter) and 0.5 (the cross-layer window-to-window connection strength parameter), the latter to allow heterogeneity in window-to-window mental states¹⁷⁴.

ROI-level variability in functional organization was estimated using the 'flexibility' function in the NCT as the number of times a given ROI changed functional communities between two consecutive windows. To account for the near degeneracy of the modularity landscape¹⁷⁸, the multilayer community detection algorithm was initiated 100 times and the ROI-level variability indices were averaged across all iterations.

Specificity analyses. To probe the specificity of any observed relationships between TSV/FCV and reproductive aging, we included four additional functional connectivity indices that fluctuate with age^{179–182}, but that we hypothesized to be more weakly associated with adjustment to environmental challenges. First, using the NCT, we estimated two ROI-specific dynamic indices: functional network segregation (called 'recruitment' in the NCT), operationalized as the number of times a given ROI was assigned to the same community as the other ROIs in its native functional system, versus functional network integration, operationalized as the number of times a given ROI was assigned to the same community as ROIs from different functional systems. In both instances, the native functional system was the one defined in the Schaefer functional atlas. Second, we applied the 'participation_coef_sign.m' function from the Brain Connectivity Toolbox¹⁸³ to the participant-specific ROI-to-ROI static correlation matrices. The participation coefficients thus estimated reflect the diversity of an ROI's connections (that is, the likelihood that an ROI has positive versus negative connections equally distributed across ROIs from all the functional systems defined in the Schaefer atlas). Participation coefficients of higher value indicate a less differentiated pattern of positive and/or negative functional connectivity.

Disorder-specific FCV maps

An overview of the contributing samples is presented in Table 2. Details on participant compensation have not been publicly released for these samples. The FCV and GMV loss maps for psychosis were based on data from the Human Connectome Project–Early Psychosis (HCP-EP), Data Release 1.1. Informed consent was obtained from the participants or their legal authorized representative/guardian in accordance with the guidelines of the local research ethics review boards across the four participating sites (Indiana University, Beth Israel Deaconess Medical Center–Massachusetts Mental Health Center, McLean Hospital and Massachusetts General Hospital).

The FCV data for MDD were taken from the Perturbation of the Depression Connectome (PDC) Project because, to our knowledge, this is the largest publicly available database of depressed patients with high-quality rfMRI data. However, due to a lack of an appropriate healthy control group (the control group for the PDC overlaps with the HCP-A sample), we estimated MDD-specific atrophy maps with data from the Kansas Musical Depression Study^{184,185} and the Russia fMRI Depression Study^{186,187}. Informed consent was obtained from all participants in the MDD studies in accordance with the guidelines of the local research ethics review boards (University of California Los Angeles (PDC), University of Kansas Medical Center (Kansas Musical Depression Study) and the multi-profile clinic Pretor/International Institute of Psychology and Psychotherapy (Novosibirsk, Russia) (Russia fMRI Depression Study)).

FCV maps

The rfMRI data for both the PDC (two resting-state runs, each lasting ~6 min and 30 s) and the HCP-EP (four resting-state runs, each lasting

-5 min and 30 s) were collected with the same parameters as for the HCP-A sample. Half of the runs for each sample were acquired with an AP-phase encoding sequence and the other half with a PA-phase encoding sequence. Our analyses featured both PDC runs and combined data from the HCP-EP to amount to the same duration as in the PDC and with an equal number of scans acquired with an AP- versus PA-phase encoding sequence. The data from both samples were preprocessed with the same pipeline described for the HCP-A sample and run through the same analytic steps described for the ABCD/HCP-A data above, to obtain ROI-specific FCV indices. We focused only on FCV because, of the two brain variability indices scrutinized, it was the only one to show a robust association with reproductive maturation/senescence.

In the PDC, before any treatment intervention, depressive symptom severity was assessed with the Hamilton Depression Rating Scale¹⁸⁸ (HDRS), which is one of the most widely used clinician-administered rating scales for primary depression. In the HCP-EP, psychosis severity was measured with the Positive and Negative Syndrome Scale¹⁸⁹ (PANSS). Disorder-specific FCV maps were estimated by computing the Spearman's partial correlation between the total HDRS score at baseline (MDD) or the total PANSS score (psychosis) and ROI-specific FCV indices across all participants, controlling for age, average relative scan-to-scan displacement, gender (both samples) and, additionally, in the HCP-EP only, also site, race (white versus non-white) and antipsychotic medication dosage. The two disorder-specific maps were standardized, then a difference map was created by subtracting the psychosis-FCV map from the MDD-FCV map. Thus, in the MDD/psychosis difference map, higher values typify ROIs that are relatively more sensitive to MDD symptoms, and lower values typify ROIs relatively more sensitive to psychotic symptoms.

Relevance to subclinical depression scores. To test whether the MDD/psychosis difference map could differentiate between subclinical variations in depressive versus non-depressive symptoms, we focused on the 440 ABCD and 130 HCP-A participants included in our main analyses who had available data on the DSM-oriented depression, anxiety, attention deficit hyperactivity disorder (ADHD) and antisocial personality and somatic disorder from the Child Behavior Checklist¹⁹⁰ and Adult Self-Report¹⁹⁰. We thus took the following steps: (1) separately, within each sample, using the confounders listed under 'Control variables', we computed partial Spearman's correlations between each ROI's FCV and DSM-oriented scores on depression, anxiety, ADHD, antisocial personality disorder and somatic disorder; (2) the resulting five DSM disorder-FCV partial correlation maps for each sample were standardized and then averaged for the corresponding disorders across the two samples; (3) a CCA with tenfold cross-validation probed the association between the MDD-psychosis-FCV difference map and the five DSM disorder-FCV partial correlation maps averaged across the ABCD and HCP-A samples.

The results of the above-mentioned CCAs, which are depicted in Supplementary Fig. 10, suggest that FCV differences linked to subclinical depression differentially map onto the MDD-FCV, rather than the psychosis-FCV, map. Complementarily, subclinical variations in anxiety and ADHD symptoms mapped onto the psychosis, rather than the MDD, FCV map. Although the MDD/psychosis difference map seems capable of differentiating between depressive and non-depressive symptoms, we note that the goal of the neuropathology CCA analyses presented in the main text was to investigate whether the brain differences linked to faster reproductive aging and perceived hostility/pain would resemble the brain profiles observed in MDD and psychosis, suggestive of likely future risk for these disorders, but not necessarily linked to the current presence of symptoms relevant to either disorder.

GMV loss maps

Disorder-specific atrophy maps were created using the exact pipelines described in refs. 191,192. Each clinical disorder group (MDD,

psychosis) was compared against demographically matched healthy controls using a two-sample *t*-test. Following extant practices in the literature¹⁹³, the group *t*-maps for each disorder were averaged and parcellated in the MNI-152 space based on the Schaefer/Gordon atlas using the 'Parcellater' function from neuromaps¹⁹⁴ (<https://github.com/netneurolab/neuromaps>) implemented in Python 3. Similar to the FCV maps, the two disorder-specific GMV maps were standardized, then a difference map was created by subtracting the psychosis GMV map from the MDD GMV map. Thus, in the MDD/psychosis difference map, higher values typify ROIs that are relatively more sensitive to MDD symptoms, whereas lower values typify ROIs that are relatively more sensitive to psychotic symptoms.

Receptor density maps relevant to reproductive aging

We analyzed receptor densities for DA, 5-HT, GLU and GABA, because these neurotransmitter systems are under substantial gonadal hormone modulation. We estimated receptor density with the normative atlas established by ref. 193, which is based on positron emission tomography (PET) data from over 1,200 healthy individuals. For each DA, GABA, GLU and 5-HT tracer map we downloaded group-averaged preprocessed PET images from https://github.com/netneurolab/hansen_receptors/tree/main/data/PET_nifti_images. The 'Parcellater' function from neuromaps¹⁹⁴ segmented each tracer map in the MNI-152 space based on the Schaefer atlas. An adapted version of the 'make_receptor_matrix.py' script (https://github.com/netneurolab/hansen_receptors/tree/main/code) from ref. 193 was used to estimate the weighted average of the receptor density maps corresponding to DA, GABA, GLU and 5-HT in Python 3. We did this separately for each tracer, taking into account the number of participants in the respective study, as implemented in ref. 193.

As in ref. 193, group-level estimates of receptor density were obtained for each of the Schaefer ROIs then standardized across all the parcels in the Schaefer atlas. To avoid biasing the canonical correlation analyses results towards the 5-HT density maps, we averaged the standardized scores corresponding to the four moderately correlated 5-HT receptor maps (HT1a, HT2, HT4 and HT6; *r* values from 0.28 to 0.57), but kept the HT1b density index separate.

Statistical analysis

CCA and PLS^{195,196} were selected to probe the relationships among our variables of interest. Given its superior performance in datasets containing highly correlated within-set variables^{197,198}, PLS was used to test the relationship of reproductive aging and stress susceptibility with ROI-level functional variability (TSV, FCV). In contrast, because of its greater sensitivity to cross-set relationships¹⁹⁸, CCA was selected to characterize the relevance of functional brain variability to both the chemoarchitecture and disorder-specific neuropathology. All CCA and PLS models were cross-validated using a tenfold procedure, then 99% CIs for each correlation coefficient (CCA) and loading/salience (PLS) were obtained by using the 'bootci' function in MATLAB (with default settings and 100,000 bootstrap samples).

PLS analysis. The MATLAB PLS toolbox was downloaded from <https://github.com/McIntosh-Lab/PLS/>. PLS was run separately in the ABCD and HCP-A samples, respectively. In these analyses, the 'behavioral' set included the reproductive maturation (ABCD)/aging (HCP-A) measures, as well as self-reported pain and perceived hostility from others (both samples). The brain matrix contained the ROI-specific TSV and FCV indices, aggregated across all available resting-state scans at each scrutinized time point (ABCD: baseline/T1, two-year follow-up/T2; HCP-A: one time point). The discovery PLS analyses in the ABCD sample contained four separate conditions (Time-1 TSV, Time-2 TSV, Time-1 FCV and Time-2 FCV). These conditions were intended to elucidate the temporal stability of the brain-reproductive aging relationship (at Time 1 and Time 2, respectively) and the potential longitudinal

relationship between the Time-1 TSV/FCV measures and the Time-2 measures of pain and/or hostility. Due to data availability, the discovery PLS analyses in the HCP-A sample contained only two conditions (TSV and FCV). In addition to the two aforementioned ‘behavioral PLS’ analyses, we ran a group (task) PLS analysis to identify age-group-related differences in brain variability patterns and test whether they could account for the observed relationships between the accelerated reproductive-aging FCV and chemoarchitectural/neuropathological maps. The group PLS analysis only featured the ROI-specific FCV data for which an association with reproductive aging had been identified (cf. Figs. 2 and 3 and Supplementary Figs. 2 and 3).

Significance and generalizability testing. The significance of the extracted brain–behavioral LV pairs was estimated through permutation testing (100,000 permutations, 200 times larger than the guidelines provided by ref. 199) in the discovery PLS analysis, which was conducted separately in the ABCD and HCP-A samples. The generalizability of our PLS models was tested using a tenfold cross-validation procedure. Specifically, the PLS analysis was run on nine folds of data, and the weights associated with the identified brain LVs were used to compute the predicted value of the brain LV in the test fold. This procedure was repeated until each of the ten folds served as ‘test data’ once. The significance of the correlation between the predicted brain LV score and the behavioral variables with which it was found to be reliably associated (see below) was estimated in the test fold using permutation-based testing with 100,000 samples.

Reliability testing. In the discovery PLS analyses, we used 100,000 bootstrap samples (that is, 1,000 times larger than the guidelines provided by ref. 199) to (1) identify ROIs making a reliable contribution to the identified LV (that is, BSRs, ROI weight/standard deviation, greater than 2 in absolute value^{200,201}, which approximate a 95% CI) and (2) estimate 95% CIs for the correlation between the ‘behavioral’ variables and the extracted brain LV¹⁹⁹. In the cross-validation procedure, we used the ‘bootci’ function in MATLAB (with default settings and 100,000 bootstraps) to characterize the (1) 99% CIs of the correlation coefficient corresponding to each ROI-level TSV/FCV and the scores of the associated LV (estimated in the test fold) and (2) 95% CIs for the correlations between the predicted value of the brain LV and the observed value of the variables in the ‘behavioral’ set¹⁹⁹.

Mediation analysis. To test whether patterns of functional brain variability account for the shared variance between accelerated biological aging and stress susceptibility, we combined the data from the two samples and conducted one mediation analysis using generalized maximum likelihood estimation in MPLUS 8.10 (ref. 202). Accelerated reproductive aging and functional brain variability (that is, FCV, based on the output of the PLS cross-validation analyses; ‘Results’) constituted the predictor and mediator variables, respectively. Susceptibility to pain and hostility, respectively, represented the two parallel outcomes. The mediation model was tested with 95% CIs estimated with 100,000 bootstrapping samples. As recommended in the literature^{82,203} bootstrapping-based 95% CIs for the indirect effects were used as effect size estimates. Although we report bias-corrected bootstrapping-based results, we verified that identical indirect effect estimates would be obtained with percentile bootstrap CIs.

CCA. To probe the relationship between functional brain variability and disorder-specific FCV (1map (MDD–psychosis)) and atrophy (1map (MDD–psychosis)), as well as receptor density maps (seven receptor density maps), we conducted a series of CCAs with cross-validation¹⁹⁵. CCA was implemented in MATLAB using the ‘canoncorr’ module. As recommended in ref. 195, we ran all CCAs on sample sizes more than ten times greater than the number of contributing variables. To evaluate the performance of our CCA-derived models, we employed a tenfold

cross-validation procedure. For all sets of CCAs, discovery analyses were conducted on nine folds of data and the resulting CCA weights were employed to derive predicted values of the brain variability and disorder-specific atrophy/receptor density variate in the left-out (‘test’) fold. This procedure was repeated until each of the ten folds served as ‘test data’ once. The 10 test folds were concatenated and the correlation between the predicted variates across the full sample was evaluated using a permutation test with 100,000 samples.

We described the relationships between measured variables and their corresponding CCA-derived variate through correlations between the observed value of a given variable and the predicted value of its corresponding variate across all test folds. Standardized canonical coefficients were not included because the unique association between a given variable and its corresponding variate was of limited value in the case of our present analyses.

The 99% CIs for each correlation coefficient were obtained by using the ‘bootci’ function in MATLAB (with default settings and 100,000 bootstrap samples). The CIs were selected to match those used in the PLS analyses, for which clearer guidelines exist (‘PLS analysis’). The aforementioned correlation coefficients are a more conservative estimate of the traditional canonical loadings as they are estimated in the test, rather than discovery, folds.

To account for correlated disorder-specific atrophy/receptor density patterns based on anatomical proximity²⁰⁴, we used Vasa’s ‘rotate_parcellation’ function in MATLAB (https://github.com/frantisekvasa/rotate_parcellation/commit/bb8b0ef10980f162793cc-180cef371e83655c505) to generate 100,000 spatially constrained permutations of the Schaefer brain LVs, as identified in the behavioral PLS analyses for the ABCD and HCP-A samples, respectively. These spatially constrained permuted functional-brain LVs were used to assess the significance of the correlation between the Schaefer brain LV and the disorder-specific atrophy/receptor density variates.

Control variables

To maximize the interpretability of the model estimates, the discovery PLS analyses were conducted on data that had not been residualized for the confounders listed below. To demonstrate the robustness of our results, the PLS cross-validation and the mediation analyses controlled for the following variables that were of no interest in the present study: (1) chronological age, to ensure that the reported inter-relationships among accelerated reproductive aging, functional brain variability, pain and hostility hold irrespective of the participants’ chronological age; (2) handedness (coded as ‘0’ for right-handedness and ‘1’ for non-right-handedness), to control for potential differences in the lateralization of the observed effects (for example, refs. 205,206); (3) serious medical problems based on the ABCD Parent Medical History Questionnaire (ABCD) or self-reported habitual use of medications, lifetime history of traumatic brain injury and body mass index as a proxy for cardiometabolic health (HCP-A), given their potential to influence BOLD signal (variability)^{207,208}; (4) socioeconomic status based on (family) income-to-needs (dependents) in both samples and years of education (HCP-A only), because it can impact reproductive aging, particularly pubertal timing¹; (5) scanner site, to account for scanner-related differences, as well as broad differences in family education and socioeconomic status across sites²⁰⁹; (6) race (HCP-A only), because it can impact reproductive senescence¹⁴⁹; (7) average modality-specific (that is, resting state) motion per participant, because it can adversely impact functional connectivity metrics, in our case FCV²¹⁰. Thus, the models derived from the ABCD and HCP-A data through the discovery PLS analyses were cross-validated via partial correlation analyses (brain LV–behavior (Figs. 2a and 3a) and brain LV–individual ROIs (Figs. 2b and 3b)), which controlled for the above confounders. Similarly, before the mediation analysis, the variables of interest were residualized for the above confounders separately within each sample.

Reporting summary

Further information on research design is available in the Nature Portfolio Reporting Summary linked to this Article.

Data availability

The raw data are available to researchers working at institutions recognized by NIMH at <https://nda.nih.gov/abcd> (ABCD), <https://nda.nih.gov/ccf/lifespan-studies> (HCP-A) and <https://nda.nih.gov/ccf/disease-studies> (PDC, HCP-EP) following completion of the relevant data-use agreements. Researchers with different affiliations need to complete separate data-use agreements, signed by an authorized signing official from their respective institutions prior to submission to the NDA. Researchers need to create an account on <https://nda.nih.gov/>. Access is typically granted within a month from submitting the data-access request via the NDA site. Access to these data is controlled due to the highly sensitive nature of the data. The MDD datasets contributing to the neuropathology GMV analyses are freely available on OpenNeuro (<https://openneuro.org/datasets/ds000171/versions/00001>; <https://openneuro.org/datasets/ds002748/versions/1.0.5>). The ABCD data repository grows and changes over time. The ABCD data used in this report came from the Adolescent Brain Cognitive Development (ABCD) Study Annual Release 4.0 #1299. DOIs can be found at <https://doi.org/10.15154/1523041>. The HCP-A data used in this report came from Annual Release 2.0 (NDA Collection ID 2847), <https://doi.org/10.15154/1520707>. The HCP-EP (NDA Collection ID 2914) 1.1 Release data used in this report came from <https://doi.org/10.15154/1522899>. The PDC data (NDA Collection ID 2844) used in this report came from Data Release 1.0, <https://doi.org/10.15154/1528673>. With regard to brain atlases, the Schaefer atlas can be downloaded from <https://github.com/ThomasYeoLab/CBIG> and the Gordon atlas can be downloaded from <https://wustl.app.box.com/v/parcels-release>. The specific dataset (ABCD, HCP-A, HCP-EP, PDC) used in this report can be accessed via the NDA site at <https://doi.org/10.15154/g3hb-nf28>.

Code availability

This study used several open-access software packages, for which we provide download links in the following. Additional preprocessing of the ABCD data was conducted in FSL (FMRIB Software Library) version 6.01 (https://fsl.fmrib.ox.ac.uk/fsl/downloads_registration/). Preprocessing of the gray-matter volume maps was conducted with Statistical Parametric Mapping software (SPM12, <http://www.fil.ion.ucl.ac.uk/spm/software/spm12>) in MATLAB v9.8. All the remaining MATLAB-based analyses were conducted in v24.10. Preprocessing of the HCP-EP and additional preprocessing of the HCP-A and PDC datasets were performed with functions from the Connectome Workbench (<https://www.humanconnectome.org/software/get-connectome-workbench>). The network-level analyses were conducted with the MATLAB-based Network Community Toolbox (<https://commdetect.weebly.com/>) and the Brain Connectivity Toolbox (<https://sites.google.com/site/bctnet/>). The MATLAB-based PLS toolbox was downloaded from <https://github.com/McIntosh-Lab/PLS/54>. CCAs, simple and partial correlation analyses were performed in MATLAB v24.10. Permutation testing for the cross-validation of the PLS model was conducted with the Permutation Analysis of Linear Models software package (PALM alpha16, <https://github.com/andersonwinkler/PALM>). The receptor density analyses were performed in Python 3 (<https://www.python.org/downloads/>) with functions from neuromaps (<https://github.com/netneurolab/neuromaps>), as well as with custom code developed by the authors of the normative chemoarchitectural atlas used in our analyses (https://github.com/netneurolab/hansen_receptors/tree/main). The spatial null maps used to cross-validate the correlation between the CCA variates (CCAs 1–6) were generated with the script downloaded from https://github.com/frantisekvasa/rotate_parcellation/commit/bb8b0ef10980f162793cc180cef371e83655c505. The mediation analyses were conducted in MPLUS v8.9 using the freely available version (<https://www.statmodel.com/demo.shtml>). ROI-level

images were created with the MATLAB-based Brain Eigenmodes toolbox, which can be downloaded from https://github.com/BMHLab/BrainEigenmodes_Legacy. Network-level results were plotted using functions from the tidyverse R package (v4.3.2; <https://github.com/tidyverse/tidyverse>). No source data are included.

References

- Colich, N. L., Rosen, M. L., Williams, E. S. & McLaughlin, K. A. Biological aging in childhood and adolescence following experiences of threat and deprivation: a systematic review and meta-analysis. *Psychol. Bull.* **146**, 721–764 (2020).
- Dehestani, N., Whittle, S., Vijayakumar, N. & Silk, T. J. Developmental brain changes during puberty and associations with mental health problems. *Dev. Cogn. Neurosci.* **60**, 101227 (2023).
- Joffe, H. et al. Impact of estradiol variability and progesterone on mood in perimenopausal women with depressive symptoms. *J. Clin. Endocrinol. Metab.* **105**, e642–e650 (2020).
- MacSweeney, N. et al. The role of brain structure in the association between pubertal timing and depression risk in an early adolescent sample (the ABCD Study(R)): a registered report. *Dev. Cogn. Neurosci.* **60**, 101223 (2023).
- Petrican, R. et al. Pubertal timing and functional neurodevelopmental alterations independently mediate the effect of family conflict on adolescent psychopathology. *Dev. Cogn. Neurosci.* **52**, 101032 (2021).
- Tao, Y. et al. Epigenetic regulation of beta-endorphin synthesis in hypothalamic arcuate nucleus neurons modulates neuropathic pain in a rodent pain model. *Nat. Commun.* **14**, 7234 (2023).
- Nahman-Averbuch, H. et al. Alterations in pain during adolescence and puberty. *Trends Neurosci.* **46**, 307–317 (2023).
- Suss, H. & Ehrlert, U. Psychological resilience during the perimenopause. *Maturitas* **131**, 48–56 (2020).
- Suss, H., Willi, J., Grub, J. & Ehrlert, U. Estradiol and progesterone as resilience markers? Findings from the Swiss Perimenopause Study. *Psychoneuroendocrinology* **127**, 105177 (2021).
- Barth, C., Villringer, A. & Sacher, J. Sex hormones affect neurotransmitters and shape the adult female brain during hormonal transition periods. *Front. Neurosci.* **9**, 37 (2015).
- Berridge, C. W., Martin, A. J., Hupalo, S. & Nicol, S. E. Estrus cycle-dependent working memory effects of prefrontal cortex corticotropin-releasing factor neurotransmission. *Neuropsychopharmacology* **47**, 2016–2023 (2022).
- Guerreiro, S. R. et al. Chronic pain causes tau-mediated hippocampal pathology and memory deficits. *Mol. Psychiatry* **27**, 4385–4393 (2022).
- Kommaddi, R. P. et al. Sex difference in evolution of cognitive decline: studies on mouse model and the Dominantly Inherited Alzheimer Network cohort. *Transl. Psychiatry* **13**, 123 (2023).
- Lopes, S. et al. Tau protein is essential for stress-induced brain pathology. *Proc. Natl Acad. Sci. USA* **113**, E3755–E3763 (2016).
- Dong, L., Teh, D. B. L., Kennedy, B. K. & Huang, Z. Unraveling female reproductive senescence to enhance healthy longevity. *Cell Res.* **33**, 11–29 (2023).
- McLaughlin, K. A., Colich, N. L., Rodman, A. M. & Weissman, D. G. Mechanisms linking childhood trauma exposure and psychopathology: a transdiagnostic model of risk and resilience. *BMC Med.* **18**, 96 (2020).
- Mahadevan, A. S., Tooley, U. A., Bertolero, M. A., Mackey, A. P. & Bassett, D. S. Evaluating the sensitivity of functional connectivity measures to motion artifact in resting-state fMRI data. *Neuroimage* **241**, 118408 (2021).
- Hastings, W. J., Shalev, I. & Belsky, D. W. Comparability of biological aging measures in the National Health and Nutrition Examination Study, 1999–2002. *Psychoneuroendocrinology* **106**, 171–178 (2019).

19. Rickard, I. J., Frankenhuys, W. E. & Nettle, D. Why are childhood family factors associated with timing of maturation? A role for internal prediction. *Perspect. Psychol. Sci.* **9**, 3–15 (2014).
20. McTeague, L. M. et al. Identification of common neural circuit disruptions in cognitive control across psychiatric disorders. *Am. J. Psychiatry* **174**, 676–685 (2017).
21. Hampel, H. et al. The foundation and architecture of precision medicine in neurology and psychiatry. *Trends Neurosci.* **46**, 176–198 (2023).
22. Lopez, M. et al. The social ecology of childhood and early life adversity. *Pediatr. Res.* **89**, 353–367 (2021).
23. Bath, K. G. Synthesizing views to understand sex differences in response to early life adversity. *Trends Neurosci.* **43**, 300–310 (2020).
24. Mogil, J. S. Sex differences in pain and pain inhibition: multiple explanations of a controversial phenomenon. *Nat. Rev. Neurosci.* **13**, 859–866 (2012).
25. Oram, S., Khalifeh, H. & Howard, L. M. Violence against women and mental health. *Lancet Psychiatry* **4**, 159–170 (2017).
26. Ho, T. C., Gifuni, A. J. & Gotlib, I. H. Psychobiological risk factors for suicidal thoughts and behaviors in adolescence: a consideration of the role of puberty. *Mol. Psychiatry* **27**, 606–623 (2022).
27. Shanley, M. R. et al. Estrous cycle mediates midbrain neuron excitability altering social behavior upon stress. *J. Neurosci.* **43**, 736–748 (2023).
28. Levine, M. E. Modeling the rate of senescence: can estimated biological age predict mortality more accurately than chronological age?. *J. Gerontol. A* **68**, 667–674 (2013).
29. Sumner, J. A., Colich, N. L., Uddin, M., Armstrong, D. & McLaughlin, K. A. Early experiences of threat, but not deprivation, are associated with accelerated biological aging in children and adolescents. *Biol. Psychiatry* **85**, 268–278 (2019).
30. Bonifacino, T. et al. Changes at glutamate tripartite synapses in the prefrontal cortex of a new animal model of resilience/vulnerability to acute stress. *Transl. Psychiatry* **13**, 62 (2023).
31. DiSabato, D. J. et al. Interleukin-1 receptor on hippocampal neurons drives social withdrawal and cognitive deficits after chronic social stress. *Mol. Psychiatry* **26**, 4770–4782 (2021).
32. Forkmann, K., Wiech, K., Schmidt, K., Schmid-Kohler, J. & Bingel, U. Neural underpinnings of preferential pain learning and the modulatory role of fear. *Cereb. Cortex* **33**, 9664–9676 (2023).
33. Choi, T.-Y. et al. Distinct prefrontal projection activity and transcriptional state conversely orchestrate social competition and hierarchy. *Neuron* <https://doi.org/10.1016/j.neuron.2023.11.012> (2023).
34. Kim, J., Kang, S., Choi, T. Y., Chang, K. A. & Koo, J. W. Metabotropic glutamate receptor 5 in amygdala target neurons regulates susceptibility to chronic social stress. *Biol. Psychiatry* **92**, 104–115 (2022).
35. Willmore, L., Cameron, C., Yang, J., Witten, I. B. & Falkner, A. L. Behavioural and dopaminergic signatures of resilience. *Nature* **611**, 124–132 (2022).
36. Menken, M. S. et al. Longitudinal alterations in brain morphometry mediated the effects of bullying victimization on cognitive development in preadolescents. *Dev. Cogn. Neurosci.* **61**, 101247 (2023).
37. Wong, T. Y. et al. Traumatic stress load and stressor reactivity score associated with accelerated gray matter maturation in youths indexed by normative models. *Mol. Psychiatry* **28**, 1137–1145 (2023).
38. Holm, M. C. et al. Linking brain maturation and puberty during early adolescence using longitudinal brain age prediction in the ABCD cohort. *Dev. Cogn. Neurosci.* **60**, 101220 (2023).
39. Thijssen, S., Collins, P. F. & Luciana, M. Does pubertal stage mediate the association between family environment and structure and function of the amygdala-mPFC circuit? A replication study of the longitudinal ABCD cohort. *Dev. Cogn. Neurosci.* **56**, 101120 (2022).
40. Vijayakumar, N., Whittle, S. & Silk, T. J. Corticolimbic connectivity mediates the relationship between pubertal timing and mental health problems. *Psychol. Med.* **53**, 7655–7665 (2023).
41. Dhamala, E., Yeo, B. T. T. & Holmes, A. J. One size does not fit all: methodological considerations for brain-based predictive modeling in psychiatry. *Biol. Psychiatry* **93**, 717–728 (2023).
42. Ooi, L. Q. R. et al. Comparison of individualized behavioral predictions across anatomical, diffusion and functional connectivity MRI. *Neuroimage* **263**, 119636 (2022).
43. Garrett, D. D. et al. Lost dynamics and the dynamics of loss: longitudinal compression of brain signal variability is coupled with declines in functional integration and cognitive performance. *Cereb. Cortex* **31**, 5239–5252 (2021).
44. Garrett, D. D., Epp, S. M., Kleemeyer, M., Lindenberger, U. & Polk, T. A. Higher performers upregulate brain signal variability in response to more feature-rich visual input. *Neuroimage* **217**, 116836 (2020).
45. Grady, C. L. & Garrett, D. D. Brain signal variability is modulated as a function of internal and external demand in younger and older adults. *Neuroimage* **169**, 510–523 (2018).
46. Padmanabhan, K. & Urban, N. N. Intrinsic biophysical diversity decorrelates neuronal firing while increasing information content. *Nat. Neurosci.* **13**, 1276–1282 (2010).
47. Petrican, R., Graham, K. S. & Lawrence, A. D. Brain-environment alignment during movie watching predicts fluid intelligence and affective function in adulthood. *Neuroimage* **238**, 118177 (2021).
48. Mujica-Parodi, L. R. et al. Diet modulates brain network stability, a biomarker for brain aging, in young adults. *Proc. Natl Acad. Sci. USA* **117**, 6170–6177 (2020).
49. Sporns, O. & Betzel, R. F. Modular brain networks. *Annu. Rev. Psychol.* **67**, 613–640 (2016).
50. Stanford, W. C., Mucha, P. J. & Dayan, E. A robust core architecture of functional brain networks supports topological resilience and cognitive performance in middle- and old-aged adults. *Proc. Natl Acad. Sci. USA* **119**, e2203682119 (2022).
51. Sydnor, V. J. et al. Intrinsic activity development unfolds along a sensorimotor-association cortical axis in youth. *Nat. Neurosci.* **26**, 638–649 (2023).
52. Graff, K. et al. Functional connectomes become more longitudinally self-stable, but not more distinct from others, across early childhood. *Neuroimage* **258**, 119367 (2022).
53. Lei, T. et al. Progressive stabilization of brain network dynamics during childhood and adolescence. *Cereb. Cortex* **32**, 1024–1039 (2022).
54. Sastry, N. C., Roy, D. & Banerjee, A. Stability of sensorimotor network sculpts the dynamic repertoire of resting state over lifespan. *Cereb. Cortex* **33**, 1246–1262 (2023).
55. Sun, L. et al. Functional connectome through the human life span. Preprint at bioRxiv <https://doi.org/10.1101/2023.09.12.557193> (2023).
56. Kaufmann, T. et al. Common brain disorders are associated with heritable patterns of apparent aging of the brain. *Nat. Neurosci.* **22**, 1617–1623 (2019).
57. Solmi, M. et al. Meta-analytic prevalence of comorbid mental disorders in individuals at clinical high risk of psychosis: the case for transdiagnostic assessment. *Mol. Psychiatry* **28**, 2291–2300 (2023).
58. Constantinides, C. et al. Brain ageing in schizophrenia: evidence from 26 international cohorts via the ENIGMA Schizophrenia consortium. *Mol. Psychiatry* **28**, 1201–1209 (2023).

59. Han, L. K. M. et al. Brain aging in major depressive disorder: results from the ENIGMA major depressive disorder working group. *Mol. Psychiatry* **26**, 5124–5139 (2021).
60. Luo, Y., Chen, W., Qiu, J. & Jia, T. Accelerated functional brain aging in major depressive disorder: evidence from a large scale fMRI analysis of Chinese participants. *Transl. Psychiatry* **12**, 397 (2022).
61. Solmi, M. et al. Age at onset of mental disorders worldwide: large-scale meta-analysis of 192 epidemiological studies. *Mol. Psychiatry* **27**, 281–295 (2022).
62. Zhu, J. D., Wu, Y. F., Tsai, S. J., Lin, C. P. & Yang, A. C. Investigating brain aging trajectory deviations in different brain regions of individuals with schizophrenia using multimodal magnetic resonance imaging and brain-age prediction: a multicenter study. *Transl. Psychiatry* **13**, 82 (2023).
63. Laube, C., van den Bos, W. & Fandakova, Y. The relationship between pubertal hormones and brain plasticity: implications for cognitive training in adolescence. *Dev. Cogn. Neurosci.* **42**, 100753 (2020).
64. Yoest, K. E., Quigley, J. A. & Becker, J. B. Rapid effects of ovarian hormones in dorsal striatum and nucleus accumbens. *Horm. Behav.* **104**, 119–129 (2018).
65. Abbasi, S., Wolff, A., Catal, Y. & Northoff, G. Increased noise relates to abnormal excitation-inhibition balance in schizophrenia: a combined empirical and computational study. *Cereb. Cortex* **33**, 10477–10491 (2023).
66. Bustillo, J. R. et al. Glutamatergic and neuronal dysfunction in gray and white matter: a spectroscopic imaging study in a large schizophrenia sample. *Schizophr. Bull.* **43**, 611–619 (2017).
67. Frankle, W. G., Himes, M., Mason, N. S., Mathis, C. A. & Narendran, R. Prefrontal and striatal dopamine release are inversely correlated in schizophrenia. *Biol. Psychiatry* **92**, 791–799 (2022).
68. Gaebler, A. J. et al. Functional connectivity signatures of NMDAR dysfunction in schizophrenia-integrating findings from imaging genetics and pharmaco-fMRI. *Transl. Psychiatry* **13**, 59 (2023).
69. Hou, C. et al. Spatiotemporal dynamics of functional connectivity and association with molecular architecture in schizophrenia. *Cereb. Cortex* **33**, 9095–9104 (2023).
70. Lu, C. et al. Atypical antipsychotics antagonize GABA(A) receptors in the ventral tegmental area GABA neurons to relieve psychotic behaviors. *Mol. Psychiatry* **28**, 2107–2121 (2023).
71. McCutcheon, R. A., Keefe, R. S. E. & McGuire, P. K. Cognitive impairment in schizophrenia: aetiology, pathophysiology and treatment. *Mol. Psychiatry* **28**, 1902–1918 (2023).
72. Parnell, E. et al. Excitatory dysfunction drives network and calcium handling deficits in 16p11.2 duplication schizophrenia induced pluripotent stem cell-derived neurons. *Biol. Psychiatry* **94**, 153–163 (2023).
73. Simpson, E. H., Gallo, E. F., Balsam, P. D., Javitch, J. A. & Kellendonk, C. How changes in dopamine D2 receptor levels alter striatal circuit function and motivation. *Mol. Psychiatry* **27**, 436–444 (2022).
74. Erritzoe, D. et al. Brain serotonin release is reduced in patients with depression: a [¹¹C]Cimbi-36 positron emission tomography study with a d-amphetamine challenge. *Biol. Psychiatry* **93**, 1089–1098 (2023).
75. Fogaca, M. V. et al. Inhibition of GABA interneurons in the mPFC is sufficient and necessary for rapid antidepressant responses. *Mol. Psychiatry* **26**, 3277–3291 (2021).
76. Fogaca, M. V. et al. M1 acetylcholine receptors in somatostatin interneurons contribute to GABAergic and glutamatergic plasticity in the mPFC and antidepressant-like responses. *Neuropsychopharmacology* **48**, 1277–1287 (2023).
77. Lewis, C. P. et al. Altered anterior cingulate glutamatergic metabolism in depressed adolescents with current suicidal ideation. *Transl. Psychiatry* **10**, 119 (2020).
78. Prevot, T. & Sibille, E. Altered GABA-mediated information processing and cognitive dysfunctions in depression and other brain disorders. *Mol. Psychiatry* **26**, 151–167 (2021).
79. Svensson, J. E. et al. Serotonin transporter availability increases in patients recovering from a depressive episode. *Transl. Psychiatry* **11**, 264 (2021).
80. Wilke, S. A., Lavi, K., Byeon, S., Donohue, K. C. & Sohal, V. S. Convergence of clinically relevant manipulations on dopamine-regulated prefrontal activity underlying stress coping responses. *Biol. Psychiatry* **91**, 810–820 (2022).
81. Gordon, E. M. et al. Generation and evaluation of a cortical area parcellation from resting-state correlations. *Cereb. Cortex* **26**, 288–303 (2016).
82. Preacher, K. J. & Hayes, A. F. SPSS and SAS procedures for estimating indirect effects in simple mediation models. *Behav. Res. Methods Instrum. Comput.* **36**, 717–731 (2004).
83. Rucker, D. D., Preacher, K. J., Tormala, Z. L. & Petty, R. E. Mediation analysis in social psychology: current practices and new recommendations. *Soc. Personal. Psychol. Compass* **5**, 359–371 (2011).
84. Raut, R. V., Snyder, A. Z. & Raichle, M. E. Hierarchical dynamics as a macroscopic organizing principle of the human brain. *Proc. Natl Acad. Sci. USA* **117**, 20890–20897 (2020).
85. Wolff, A. et al. Intrinsic neural timescales: temporal integration and segregation. *Trends Cogn. Sci.* **26**, 159–173 (2022).
86. Lund, M. J. et al. Brain age prediction using fMRI network coupling in youths and associations with psychiatric symptoms. *Neuroimage Clin.* **33**, 102921 (2022).
87. Setton, R. et al. Age differences in the functional architecture of the human brain. *Cereb. Cortex* **33**, 114–134 (2022).
88. Kong, X. et al. Sensory-motor cortices shape functional connectivity dynamics in the human brain. *Nat. Commun.* **12**, 6373 (2021).
89. Chai, Y. et al. Functional connectomics in depression: insights into therapies. *Trends Cogn. Sci.* **27**, 814–832 (2023).
90. Javaheripour, N. et al. Altered resting-state functional connectome in major depressive disorder: a mega-analysis from the PsyMRI consortium. *Transl. Psychiatry* **11**, 511 (2021).
91. Ray, D., Bezmaternykh, D., Mel'nikov, M., Friston, K. J. & Das, M. Altered effective connectivity in sensorimotor cortices is a signature of severity and clinical course in depression. *Proc. Natl Acad. Sci. USA* **118**, e2105730118 (2021).
92. Sun, X. et al. Mapping neurophysiological subtypes of major depressive disorder using normative models of the functional connectome. *Biol. Psychiatry* **94**, 936–947 (2023).
93. Rolls, E. T., Cheng, W. & Feng, J. Brain dynamics: the temporal variability of connectivity, and differences in schizophrenia and ADHD. *Transl. Psychiatry* **11**, 70 (2021).
94. Roy, D. S. et al. Anterior thalamic dysfunction underlies cognitive deficits in a subset of neuropsychiatric disease models. *Neuron* **109**, 2590–2603.e13 (2021).
95. Constantinidis, C. & Luna, B. Neural substrates of inhibitory control maturation in adolescence. *Trends Neurosci.* **42**, 604–616 (2019).
96. Vink, M. et al. Towards an integrated account of the development of self-regulation from a neurocognitive perspective: a framework for current and future longitudinal multi-modal investigations. *Dev. Cogn. Neurosci.* **45**, 100829 (2020).
97. Spreng, R. N. & Turner, G. R. The shifting architecture of cognition and brain function in older adulthood. *Perspect. Psychol. Sci.* **14**, 523–542 (2019).
98. Spreng, R. N. & Turner, G. R. From exploration to exploitation: a shifting mental mode in late life development. *Trends Cogn. Sci.* **25**, 1058–1071 (2021).

99. Asraf, K., Zaidan, H., Natoor, B. & Gaisler-Salomon, I. Synergistic, long-term effects of glutamate dehydrogenase 1 deficiency and mild stress on cognitive function and mPFC gene and miRNA expression. *Transl. Psychiatry* **13**, 248 (2023).
100. Milosavljevic, S., Smith, A. K., Wright, C. J., Valafar, H. & Pocivavsek, A. Kynurenone aminotransferase II inhibition promotes sleep and rescues impairments induced by neurodevelopmental insult. *Transl. Psychiatry* **13**, 106 (2023).
101. Eck, S. R. & Bangasser, D. A. The effects of early life stress on motivated behaviors: a role for gonadal hormones. *Neurosci. Biobehav. Rev.* **119**, 86–100 (2020).
102. Fox, M. E. & Lobo, M. K. The molecular and cellular mechanisms of depression: a focus on reward circuitry. *Mol. Psychiatry* **24**, 1798–1815 (2019).
103. Braun, U. et al. Brain network dynamics during working memory are modulated by dopamine and diminished in schizophrenia. *Nat. Commun.* **12**, 3478 (2021).
104. Mikus, N. et al. Blocking D2/D3 dopamine receptors in male participants increases volatility of beliefs when learning to trust others. *Nat. Commun.* **14**, 4049 (2023).
105. Radley, J. J. & Herman, J. P. Preclinical models of chronic stress: adaptation or pathology? *Biol. Psychiatry* **94**, 194–202 (2023).
106. Selye, H. Stress and the general adaptation syndrome. *Br. Med. J.* **1**, 1383–1392 (1950).
107. Keyes, K. M. & Platt, J. M. Annual Research Review: sex, gender and internalizing conditions among adolescents in the 21st century - trends, causes, consequences. *J. Child Psychol. Psychiatry* **65**, 384–407 (2024).
108. de Lange, S. C. et al. Shared vulnerability for connectome alterations across psychiatric and neurological brain disorders. *Nat. Hum. Behav.* **3**, 988–998 (2019).
109. Englund, J. et al. Downregulation of kainate receptors regulating GABAergic transmission in amygdala after early life stress is associated with anxiety-like behavior in rodents. *Transl. Psychiatry* **11**, 538 (2021).
110. Mederos, S. et al. GABAergic signaling to astrocytes in the prefrontal cortex sustains goal-directed behaviors. *Nat. Neurosci.* **24**, 82–92 (2021).
111. Gallo, F. T. et al. Dopamine modulates adaptive forgetting in medial prefrontal cortex. *J. Neurosci.* **42**, 6620–6636 (2022).
112. Dupuis, J. P., Nicole, O. & Groc, L. NMDA receptor functions in health and disease: old actor, new dimensions. *Neuron* **111**, 2312–2328 (2023).
113. Bickle, J. G. et al. 5-HT_{1A} receptors on dentate gyrus granule cells confer stress resilience. *Biol. Psychiatry* <https://doi.org/10.1016/j.biopsych.2023.10.007> (2024).
114. Markova, T. Z. et al. Poorer aging trajectories are associated with elevated serotonin synthesis capacity. *Mol. Psychiatry* <https://doi.org/10.1038/s41380-023-02177-x> (2023).
115. Kipkemoi, P. et al. Phenotype and genetic analysis of data collected within the first year of NeuroDev. *Neuron* **111**, 2800–2810 (2023).
116. Humphreys, K. L. et al. DNA methylation of HPA-axis genes and the onset of major depressive disorder in adolescent girls: a prospective analysis. *Transl. Psychiatry* **9**, 245 (2019).
117. Starnawska, A. et al. Epigenome-wide association study of depression symptomatology in elderly monozygotic twins. *Transl. Psychiatry* **9**, 214 (2019).
118. Yusupov, N. et al. Transdiagnostic evaluation of epigenetic age acceleration and burden of psychiatric disorders. *Neuropsychopharmacology* **48**, 1409–1417 (2023).
119. Ferrer, A. et al. BDNF genetic variants and methylation: effects on cognition in major depressive disorder. *Transl. Psychiatry* **9**, 265 (2019).
120. Drzymalla, E. et al. Association between maternal depression during pregnancy and newborn DNA methylation. *Transl. Psychiatry* **11**, 572 (2021).
121. Kurtin, D. L., Scott, G., Hebron, H., Skeldon, A. C. & Violante, I. R. Task-based differences in brain state dynamics and their relation to cognitive ability. *Neuroimage* **271**, 119945 (2023).
122. Di, X., Xu, T., Uddin, L. Q. & Biswal, B. B. Individual differences in time-varying and stationary brain connectivity during movie watching from childhood to early adulthood: age, sex and behavioral associations. *Dev. Cogn. Neurosci.* **63**, 101280 (2023).
123. Luppi, A. I. et al. A synergistic core for human brain evolution and cognition. *Nat. Neurosci.* **25**, 771–782 (2022).
124. Pines, A. et al. Development of top-down cortical propagations in youth. *Neuron* **111**, 1316–1330 (2023).
125. Stegemann, A. et al. Prefrontal engrams of long-term fear memory perpetuate pain perception. *Nat. Neurosci.* **26**, 820–829 (2023).
126. Chu, C. et al. Total sleep deprivation increases brain age prediction reversibly in multisite samples of young healthy adults. *J. Neurosci.* **43**, 2168–2177 (2023).
127. Qin, H. et al. REM sleep-active hypothalamic neurons may contribute to hippocampal social-memory consolidation. *Neuron* **110**, 4000–4014.e6 (2022).
128. Lopez-Otin, C., Blasco, M. A., Partridge, L., Serrano, M. & Kroemer, G. Hallmarks of aging: an expanding universe. *Cell* **186**, 243–278 (2023).
129. Krivonosov, M. I. et al. A new cognitive clock matching phenotypic and epigenetic ages. *Transl. Psychiatry* **12**, 364 (2022).
130. Finger, C. E., Moreno-Gonzalez, I., Gutierrez, A., Moruno-Manchon, J. F. & McCullough, L. D. Age-related immune alterations and cerebrovascular inflammation. *Mol. Psychiatry* **27**, 803–818 (2022).
131. Granata, L., Gildawie, K. R., Ismail, N., Brenhouse, H. C. & Kopec, A. M. Immune signaling as a node of interaction between systems that sex-specifically develop during puberty and adolescence. *Dev. Cogn. Neurosci.* **57**, 101143 (2022).
132. Toenders, Y. J. et al. Inflammation and depression in young people: a systematic review and proposed inflammatory pathways. *Mol. Psychiatry* **27**, 315–327 (2022).
133. Shanmugan, S. et al. Sex differences in the functional topography of association networks in youth. *Proc. Natl Acad. Sci. USA* **119**, e2110416119 (2022).
134. Gui, Y. et al. Sex-specific genetic association between psychiatric disorders and cognition, behavior and brain imaging in children and adults. *Transl. Psychiatry* **12**, 347 (2022).
135. Maitra, M. et al. Cell type specific transcriptomic differences in depression show similar patterns between males and females but implicate distinct cell types and genes. *Nat. Commun.* **14**, 2912 (2023).
136. Dark, H. E. et al. Sex-related differences in violence exposure, neural reactivity to threat, and mental health. *Neuropsychopharmacology* **47**, 2221–2229 (2022).
137. Holloway, A. L., Schaid, M. D. & Lerner, T. N. Chronically dysregulated corticosterone impairs dopaminergic transmission in the dorsomedial striatum by sex-divergent mechanisms. *Neuropsychopharmacology* **48**, 1328–1337 (2023).
138. Salberg, S. et al. The waiting game: investigating the neurobiological transition from acute to persistent pain in adolescent rats. *Cereb. Cortex* **33**, 6382–6393 (2023).
139. Orchard, E. R., Rutherford, H. J. V., Holmes, A. J. & Jamadar, S. D. Matrescence: lifetime impact of motherhood on cognition and the brain. *Trends Cogn. Sci.* **27**, 302–316 (2023).
140. Hoekzema, E. et al. Mapping the effects of pregnancy on resting state brain activity, white matter microstructure, neural metabolite concentrations and grey matter architecture. *Nat. Commun.* **13**, 6931 (2022).

141. Puri, T. A., Richard, J. E. & Galea, L. A. M. Beyond sex differences: short- and long-term effects of pregnancy on the brain. *Trends Neurosci.* **46**, 459–471 (2023).
142. Orchard, E. R. et al. Neuroprotective effects of motherhood on brain function in late life: a resting-state fMRI study. *Cereb. Cortex* **31**, 1270–1283 (2021).
143. Pestana, J. E., Kershaw, K. A. & Graham, B. M. The impact of the ovarian cycle on anxiety, allopregnanolone and corticotropin releasing hormone changes after motherhood in female rats and women. *Transl. Psychiatry* **13**, 183 (2023).
144. Nicholas, M. K. The biopsychosocial model of pain 40 years on: time for a reappraisal? *Pain* **163**, S3–S14 (2022).
145. Senger-Carpenter, T. et al. Biopsychosocial attributes of single-region and multi-region body pain during early adolescence: analysis of the ABCD cohort. *Clin. J. Pain* **38**, 670–679 (2022).
146. King, S. et al. The epidemiology of chronic pain in children and adolescents revisited: a systematic review. *Pain* **152**, 2729–2738 (2011).
147. Rader, L., Freis, S. M. & Friedman, N. P. Associations between adolescent pain and psychopathology in the Adolescent Brain Cognitive Development (ABCD) Study. *Behav. Genet.* **53**, 232–248 (2023).
148. Bleil, M. E., Booth-LaForce, C. & Benner, A. D. Race disparities in pubertal timing: implications for cardiovascular disease risk among African American women. *Popul. Res. Policy Rev.* **36**, 717–738 (2017).
149. Harlow, S. D. et al. Disparities in reproductive aging and midlife health between black and white women: the Study of Women's Health Across the Nation (SWAN). *Womens Midlife Health* **8**, 3 (2022).
150. Hayward, C., Gotlib, I. H., Schraedley, P. K. & Litt, I. F. Ethnic differences in the association between pubertal status and symptoms of depression in adolescent girls. *J. Adolesc. Health* **25**, 143–149 (1999).
151. Sun, S. S. et al. National estimates of the timing of sexual maturation and racial differences among US children. *Pediatrics* **110**, 911–919 (2002).
152. Bookheimer, S. Y. et al. The Lifespan Human Connectome Project in Aging: an overview. *Neuroimage* **185**, 335–348 (2019).
153. Petersen, A. C., Crockett, L., Richards, M. & Boxer, A. A self-report measure of pubertal status: reliability, validity and initial norms. *J. Youth Adolesc.* **17**, 117–133 (1988).
154. Harlow, S. D. et al. Executive summary of the Stages of Reproductive Aging Workshop +10: addressing the unfinished agenda of staging reproductive aging. *Climacteric* **15**, 105–114 (2012).
155. Petrican, R., Fornito, A. & Jones, N. Psychological resilience and neurodegenerative risk: a connectomics-transcriptomics investigation in healthy adolescent and middle-aged females. *Neuroimage* **255**, 119209 (2022).
156. Karcher, N. R. & Barch, D. M. The ABCD study: understanding the development of risk for mental and physical health outcomes. *Neuropsychopharmacology* **46**, 131–142 (2021).
157. Barch, D. M. et al. Demographic and mental health assessments in the adolescent brain and cognitive development study: updates and age-related trajectories. *Dev. Cogn. Neurosci.* **52**, 101031 (2021).
158. Bolton, T. A. W., Morgenroth, E., Preti, M. G. & Van De Ville, D. Tapping into multi-faceted human behavior and psychopathology using fMRI brain dynamics. *Trends Neurosci.* **43**, 667–680 (2020).
159. Waschke, L., Kloosterman, N. A., Obleser, J. & Garrett, D. D. Behavior needs neural variability. *Neuron* **109**, 751–766 (2021).
160. Mansson, K. N. T. et al. Moment-to-moment brain signal variability reliably predicts psychiatric treatment outcome. *Biol. Psychiatry* **91**, 658–666 (2022).
161. Harms, M. P. et al. Extending the Human Connectome Project across ages: imaging protocols for the Lifespan Development and Aging projects. *Neuroimage* **183**, 972–984 (2018).
162. Hagler, D. J. Jr et al. Image processing and analysis methods for the Adolescent Brain Cognitive Development Study. *Neuroimage* **202**, 116091 (2019).
163. Fair, D. A. et al. Correction of respiratory artifacts in MRI head motion estimates. *Neuroimage* **208**, 116400 (2020).
164. Glasser, M. F. et al. The minimal preprocessing pipelines for the Human Connectome Project. *Neuroimage* **80**, 105–124 (2013).
165. Schaefer, A. et al. Local-global parcellation of the human cerebral cortex from intrinsic functional connectivity MRI. *Cereb. Cortex* **28**, 3095–3114 (2018).
166. Petrican, R. & Fornito, A. Adolescent neurodevelopment and psychopathology: the interplay between adversity exposure and genetic risk for accelerated brain ageing. *Dev. Cogn. Neurosci.* **60**, 101229 (2023).
167. Petrican, R., Fornito, A. & Boyland, E. Lifestyle factors counteract the neurodevelopmental impact of genetic risk for accelerated brain aging in adolescence. *Biol. Psychiatry* **95**, 453–464 (2024).
168. Kebets, V. et al. Fronto-limbic neural variability as a transdiagnostic correlate of emotion dysregulation. *Transl. Psychiatry* **11**, 545 (2021).
169. Garrett, D. D., Kovacevic, N., McIntosh, A. R. & Grady, C. L. The importance of being variable. *J. Neurosci.* **31**, 4496–4503 (2011).
170. Kielar, A. et al. Identifying dysfunctional cortex: dissociable effects of stroke and aging on resting state dynamics in MEG and fMRI. *Front. Aging Neurosci.* **8**, 40 (2016).
171. Braun, U. et al. Dynamic reconfiguration of frontal brain networks during executive cognition in humans. *Proc. Natl Acad. Sci. USA* **112**, 11678–11683 (2015).
172. Chen, T., Cai, W., Ryali, S., Supekar, K. & Menon, V. Distinct global brain dynamics and spatiotemporal organization of the salience network. *PLoS Biol.* **14**, e1002469 (2016).
173. Telesford, Q. K. et al. Detection of functional brain network reconfiguration during task-driven cognitive states. *Neuroimage* **142**, 198–210 (2016).
174. Finc, K. et al. Dynamic reconfiguration of functional brain networks during working memory training. *Nat. Commun.* **11**, 2435 (2020).
175. Bassett, D. S. Network Community Toolbox <http://commdetect.weebly.com> (2017).
176. Mucha, P. J., Richardson, T., Macon, K., Porter, M. A. & Onnela, J. P. Community structure in time-dependent, multiscale and multiplex networks. *Science* **328**, 876–878 (2010).
177. Mattar, M. G., Cole, M. W., Thompson-Schill, S. L. & Bassett, D. S. A functional cartography of cognitive systems. *PLoS Comput. Biol.* **11**, e1004533 (2015).
178. Good, B. H., de Montjoye, Y. A. & Clauset, A. Performance of modularity maximization in practical contexts. *Phys. Rev. E* **81**, 046106 (2010).
179. Chan, M. Y., Park, D. C., Savalia, N. K., Petersen, S. E. & Wig, G. S. Decreased segregation of brain systems across the healthy adult lifespan. *Proc. Natl Acad. Sci. USA* **111**, E4997–E5006 (2014).
180. Pedersen, R. et al. When functional blurring becomes deleterious: reduced system segregation is associated with less white matter integrity and cognitive decline in aging. *Neuroimage* **242**, 118449 (2021).
181. Schlesinger, K. J., Turner, B. O., Lopez, B. A., Miller, M. B. & Carlson, J. M. Age-dependent changes in task-based modular organization of the human brain. *Neuroimage* **146**, 741–762 (2017).
182. Yang, X. et al. Age-dependent changes in the dynamic functional organization of the brain at rest: a cross-cultural replication approach. *Cereb. Cortex* **33**, 6394–6406 (2023).

183. Rubinov, M. & Sporns, O. Complex network measures of brain connectivity: uses and interpretations. *Neuroimage* **52**, 1059–1069 (2010).
184. Lepping, R. J. et al. Neural processing of emotional musical and nonmusical stimuli in depression. *PLoS ONE* **11**, e0156859 (2016).
185. Lepping, R. J. et al. Neural processing of emotional musical and nonmusical stimuli in depression. *OpenNeuro* <https://openneuro.org/datasets/ds000171/versions/00001> (2018).
186. Bezmaternyykh, D., Melnikov, M., Savelov, A. & Petrovskii, E. Resting state with closed eyes for patients with depression and healthy participants. *OpenNeuro* <https://doi.org/10.18112/openneuro.ds002748.v1.0.5> (2020).
187. Mel'nikov, M. E. et al. fMRI response of parietal brain areas to sad facial stimuli in mild depression. *Bull. Exp. Biol. Med.* **165**, 741–745 (2018).
188. Hamilton, M. A rating scale for depression. *J. Neurol. Neurosurg. Psychiatry* **23**, 56–62 (1960).
189. Kay, S. R., Fiszbein, A. & Opler, L. A. The positive and negative syndrome scale (PANSS) for schizophrenia. *Schizophr. Bull.* **13**, 261–276 (1987).
190. Achenbach, T. M. *The Achenbach System of Empirically Based Assessment (ASEBA): Development, Findings, Theory and Applications* (Univ. Vermont, Research Center for Children, Youth and Families, 2009).
191. Segal, A. et al. Regional, circuit and network heterogeneity of brain abnormalities in psychiatric disorders. *Nat. Neurosci.* **26**, 1613–1629 (2023).
192. Chopra, S. et al. Network-based spreading of gray matter changes across different stages of psychosis. *JAMA Psychiatry* **80**, 1256–1257 (2023).
193. Hansen, J. Y. et al. Mapping neurotransmitter systems to the structural and functional organization of the human neocortex. *Nat. Neurosci.* **25**, 1569–1581 (2022).
194. Markello, R. D. et al. neuromaps: structural and functional interpretation of brain maps. *Nat. Methods* **19**, 1472–1479 (2022).
195. Hair, J. F., Black, W. C., Babin, B. J. & Anderson, R. E. *Multivariate Data Analysis* 7th edn (Pearson, 2014).
196. Krishnan, A., Williams, L. J., McIntosh, A. R. & Abdi, H. Partial Least Squares (PLS) methods for neuroimaging: a tutorial and review. *Neuroimage* **56**, 455–475 (2011).
197. McIntosh, A. R. & Misic, B. Multivariate statistical analyses for neuroimaging data. *Annu. Rev. Psychol.* **64**, 499–525 (2013).
198. Mihalik, A. et al. Canonical correlation analysis and partial least squares for identifying brain-behavior associations: a tutorial and a comparative study. *Biol. Psychiatry Cogn. Neurosci. Neuroimaging* **7**, 1055–1067 (2022).
199. McIntosh, A. R. & Lobaugh, N. J. Partial least squares analysis of neuroimaging data: applications and advances. *Neuroimage* **23**, S250–S263 (2004).
200. Mwilambwe-Tshiloblo, L., Setton, R., Bzdok, D., Turner, G. R. & Spreng, R. N. Age differences in functional brain networks associated with loneliness and empathy. *Netw. Neurosci.* **7**, 496–521 (2023).
201. Wearn, A. et al. Neuromodulatory subcortical nucleus integrity is associated with white matter microstructure, tauopathy and APOE status. *Nat. Commun.* **15**, 4706 (2024).
202. Muthén, L. K. & Muthén, B. O. MPLUS 8.10 (Muthén & Muthén, 1998–2011).
203. Miocevic, M., O'Rourke, H. P., MacKinnon, D. P. & Brown, H. C. Statistical properties of four effect-size measures for mediation models. *Behav. Res. Methods* **50**, 285–301 (2018).
204. Fornito, A., Arnatkeviciute, A. & Fulcher, B. D. Bridging the gap between connectome and transcriptome. *Trends Cogn. Sci.* **23**, 34–50 (2019).
205. Tejavibulya, L. et al. Large-scale differences in functional organization of left- and right-handed individuals using whole-brain, data-driven analysis of connectivity. *Neuroimage* **252**, 119040 (2022).
206. Tomasi, D. & Volkow, N. D. Associations between handedness and brain functional connectivity patterns in children. *Nat. Commun.* **15**, 2355 (2024).
207. Medaglia, J. D. Functional neuroimaging in traumatic brain injury: from nodes to networks. *Front. Neurol.* **8**, 407 (2017).
208. Millar, P. R. et al. Evaluating the sensitivity of resting-state BOLD variability to age and cognition after controlling for motion and cardiovascular influences: a network-based approach. *Cereb. Cortex* **30**, 5686–5701 (2020).
209. Rosenberg, M. D. et al. Behavioral and neural signatures of working memory in childhood. *J. Neurosci.* **40**, 5090–5104 (2020).
210. Power, J. D., Schlaggar, B. L. & Petersen, S. E. Recent progress and outstanding issues in motion correction in resting state fMRI. *Neuroimage* **105**, 536–551 (2015).
211. Duncan, F. E. Egg quality during the pubertal transition—is youth all it's cracked up to be? *Front. Endocrinol.* **8**, 226 (2017).

Acknowledgements

The data used in the preparation of this Article were obtained from the Adolescent Brain Cognitive Development (ABCD) Study (<https://abcdstudy.org>), the Lifespan Human Connectome Project (HCP) (<https://www.humanconnectome.org/study/hcp-lifespan-aging>), the Perturbation of the Depression Connectome (PDC, Data Release 1.0) and the Human Connectome Project-Early Psychosis (HCP-EP, Data Release 1.1), all of which are held in the NIMH Data Archive (NDA). The ABCD Study is a multisite, longitudinal study designed to recruit more than 10,000 children aged 9–10 years and follow them over ten years into early adulthood. The ABCD Study is supported by the National Institutes of Health and additional federal partners under awards nos. U01DA041048, U01DA050989, U01DA051016, U01DA041022, U01DA051018, U01DA051037, U01DA050987, U01DA041174, U01DA041106, U01DA041117, U01DA041028, U01DA041134, U01DA050988, U01DA051039, U01DA041156, U01DA041025, U01DA041120, U01DA051038, U01DA041148, U01DA041093, U01DA041089, U24DA041123 and U24DA041147. A full list of supporters is available at <https://abcdstudy.org/federal-partners.html>. A listing of participating sites and a complete listing of the study investigators can be found at https://abcdstudy.org/consortium_members/. ABCD consortium investigators designed and implemented the study and/or provided data, but did not necessarily participate in the analysis or writing of this report. The Lifespan HCP research is supported by grants U01MH109589, U01MH109589-S1, U01AG052564 and U01AG052564-S1 and by the 14 NIH institutes and centers that support the NIH Blueprint for Neuroscience Research, by the McDonnell Center for Systems Neuroscience at Washington University, by the Office of the Provost at Washington University, by the University of Minnesota Medical School, by the University of Massachusetts Medical School and by the University of California Los Angeles Medical School. Research using Human Connectome Project for Early Psychosis (HCP-EP) data reported in this publication was supported by the National Institute of Mental Health of the National Institutes of Health under award no. U01MH109977. A.F. was supported by the National Health and Medical Research Council (ID 1197431) and Australian Research Council (ID FL220100184). This manuscript reflects the views of the authors and may not reflect the opinions or views of the NIH, HCP or PDC consortium investigators. The funders had no role in study design, data collection and analysis, decision to publish or preparation of the manuscript.

Author contributions

R.P. carried out conceptualization, methodology, formal analysis, data curation, visualization and writing of the original draft. S.C. contributed methodology, formal analysis, data curation, writing, review and editing. A.S. contributed methodology, formal analysis, data curation, writing, review and editing. N.F. carried out investigations, writing, review and editing. A.F. provided conceptualization, methodology, writing, review and editing.

Competing interests

The authors declare no competing interests.

Additional information

Supplementary information The online version contains supplementary material available at <https://doi.org/10.1038/s44220-024-00352-9>.

Correspondence and requests for materials should be addressed to Raluca Petrican.

Peer review information *Nature Mental Health* thanks Niamh MacSweeney, Ioannis Pappas and Jing Sui for their contribution to the peer review of this work.

Reprints and permissions information is available at www.nature.com/reprints.

Publisher's note Springer Nature remains neutral with regard to jurisdictional claims in published maps and institutional affiliations.

Open Access This article is licensed under a Creative Commons Attribution 4.0 International License, which permits use, sharing, adaptation, distribution and reproduction in any medium or format, as long as you give appropriate credit to the original author(s) and the source, provide a link to the Creative Commons licence, and indicate if changes were made. The images or other third party material in this article are included in the article's Creative Commons licence, unless indicated otherwise in a credit line to the material. If material is not included in the article's Creative Commons licence and your intended use is not permitted by statutory regulation or exceeds the permitted use, you will need to obtain permission directly from the copyright holder. To view a copy of this licence, visit <http://creativecommons.org/licenses/by/4.0/>.

© The Author(s) 2025

Reporting Summary

Nature Portfolio wishes to improve the reproducibility of the work that we publish. This form provides structure for consistency and transparency in reporting. For further information on Nature Portfolio policies, see our [Editorial Policies](#) and the [Editorial Policy Checklist](#).

Statistics

For all statistical analyses, confirm that the following items are present in the figure legend, table legend, main text, or Methods section.

n/a Confirmed

- The exact sample size (n) for each experimental group/condition, given as a discrete number and unit of measurement
- A statement on whether measurements were taken from distinct samples or whether the same sample was measured repeatedly
- The statistical test(s) used AND whether they are one- or two-sided
Only common tests should be described solely by name; describe more complex techniques in the Methods section.
- A description of all covariates tested
- A description of any assumptions or corrections, such as tests of normality and adjustment for multiple comparisons
- A full description of the statistical parameters including central tendency (e.g. means) or other basic estimates (e.g. regression coefficient) AND variation (e.g. standard deviation) or associated estimates of uncertainty (e.g. confidence intervals)
- For null hypothesis testing, the test statistic (e.g. F , t , r) with confidence intervals, effect sizes, degrees of freedom and P value noted
Give P values as exact values whenever suitable.
- For Bayesian analysis, information on the choice of priors and Markov chain Monte Carlo settings
- For hierarchical and complex designs, identification of the appropriate level for tests and full reporting of outcomes
- Estimates of effect sizes (e.g. Cohen's d , Pearson's r), indicating how they were calculated

Our web collection on [statistics for biologists](#) contains articles on many of the points above.

Software and code

Policy information about [availability of computer code](#)

Data collection

We did not use any software to collect the data as we analysed already collected data.

Data analysis

Analyses were conducted in Matlab (v9.8, and 24.10) and Python3. Images were created with functions from R package (v4.3.2). We used the following freely available toolboxes: Network Community Toolbox (<http://commdetect.weebly.com/>), Brain Connectivity Toolbox (<https://sites.google.com/site/bctnet/>), Neuromaps (<https://netneurolab.github.io/neuromaps/usage.html>), MPlus (v8.9), FSL (v6.01), Permutation Analysis of Linear Models software package (PALM alpha116, <https://github.com/andersonwinkler/PALM>), Statistical Parametric Mapping software (SPM12, <http://www.fil.ion.ucl.ac.uk/spm/software/spm12>), the Connectome Workbench (<https://www.humanconnectome.org/software/get-connectome-workbench>), PLS (<https://github.com/McIntosh-Lab/PLS/54>), BrainEigenModes(https://github.com/BMHLab/BrainEigenmodes_legacy). Custom scripts were used to run the receptor density analyses (https://github.com/netneurolab/hansen_receptors/tree/main) and generate the spatial null maps used in the cross-validation of the multivariate models (https://github.com/frantisekvasa/rotate_parcellation/commit/bb8b0ef10980f162793cc180cef371e83655c505).

For manuscripts utilizing custom algorithms or software that are central to the research but not yet described in published literature, software must be made available to editors and reviewers. We strongly encourage code deposition in a community repository (e.g. GitHub). See the Nature Portfolio [guidelines for submitting code & software](#) for further information.

Data

Policy information about [availability of data](#)

All manuscripts must include a [data availability statement](#). This statement should provide the following information, where applicable:

- Accession codes, unique identifiers, or web links for publicly available datasets
- A description of any restrictions on data availability
- For clinical datasets or third party data, please ensure that the statement adheres to our [policy](#)

The raw data are available to researchers working at institutions recognized by NIMH at <https://nda.nih.gov/abcd> (ABCD), at <https://nda.nih.gov/ccf/lifespan-studies> (HCP-A) and at <https://nda.nih.gov/ccf/disease-studies> (PDC, HCP-EP) upon completion of the relevant data use agreements. Researchers with different affiliations need to complete separate data use agreements which are signed by an authorized signing official from their respective institutions prior to submission to the NDA. Researchers need to create an account on <https://nda.nih.gov/>. Access is typically granted within a month from submitting the data access request via the NDA site. Access to these data is controlled due to the highly sensitive nature of the data. The MDD datasets contributing to the neuropathology GMV analyses are freely available on OpenNeuro (<https://openneuro.org/datasets/ds000171/versions/00001>; <https://openneuro.org/datasets/ds002748/versions/1.0.5>). The ABCD data repository grows and changes over time. The ABCD data used in this report came from Adolescent Brain Cognitive Development Study (ABCD) - Annual Release 4.0 #1299. DOIs can be found at <http://dx.doi.org/10.15154/1523041>. The HCP-A data used in this report came the Annual Release 2.0 (NDA Collection ID 2847), DOI: 10.15154/1520707. The HCP-EP (NDA Collection ID 2914) 1.1 Release data used in this report came from DOI: 10.15154/1522899. The PDC data (NDA Collection ID 2844) used in this report came from Data Release 1.0, DOI: <http://dx.doi.org/10.15154/1528673>. With regards to brain atlases, the Schaefer atlas can be downloaded from <https://github.com/ThomasYeoLab/CBIG> and the Gordon atlas can be downloaded from <https://wustl.app.box.com/v/parcels-release>.

Human research participants

Policy information about [studies involving human research participants and Sex and Gender in Research](#).

Reporting on sex and gender

Analyses involving the ABCD/HCP-A samples only included self-reported female individuals primarily because of the availability of well-validated measures indexing stages of reproductive aging based on quantifiable factors. Likewise, the two OpenNeuro MDD datasets contained only self-reported female participants.. Analyses based on other samples (PDC, HCP-EP) controlled for self-reported sex.

Population characteristics

ABCD: 441 White female adolescents (9-12 years of age, mostly right-handed),
HCP-A: 130 women (36-60 years of age, mostly right-handed, 62% White).
PDC: 100 depressed patients (aged 20-76 years), White, both sexes, mostly right-handed ;
HCP-EP: 121 patients/57 controls (aged 16-35 years), multi-race, both sexes, handedness not reported;
Open Neuro MDD: 26 controls/48 patients (aged 18-59 years), female, right-handed

Recruitment

Described in Garavan et al., 2018 (ABCD), Bookheimer et al., 2019 (HCP-A) or on the study website/manual: <https://www.humanconnectome.org/study/human-connectome-project-for-early-psychosis> (HCP-EP), <https://www.humanconnectome.org/study/crhd-perturbation-treatment-resistant-depression-connectome-fast-acting-therapies> (PDC), <https://openneuro.org/datasets/ds000171/versions/00001> (OpenNeuro Musical Depression Study), <https://openneuro.org/datasets/ds002748/versions/1.0.5>, Bezmaternykh et al. (2021) (OpenNeuro Russia Depression Study)

Ethics oversight

The study was approved by the local ethics committee of each dataset, and written informed consent was obtained from each participant or their authorized legal representative/guardian (the latter for ABCD youth and HCP-EP patients) . For the ABCD study, the research ethics boards were Children's Hospital Los Angeles, Florida International University, Laureate Institute for Brain Research, Medical University of South Carolina, Oregon Health & Science University, SRI International, University of California San Diego, University of California Los Angeles, University of Colorado Boulder, University of Florida, University of Maryland at Baltimore, University of Michigan, University of Minnesota, University of Pittsburgh, University of Rochester, University of Utah, University of Vermont, University of Wisconsin-Milwaukee, Virginia Commonwealth University, Washington University in St. Louis and Yale university. For the HCP-A study, the local research ethics boards were University of California Los Angeles Medical School, University of Massachusetts Medical School, University of Minnesota Medical School and Washington University at St. Louis. For the HCP-EP study, the local ethics boards were Indiana University, Beth Israel Deaconess Medical Center – Massachusetts Mental Health Center, McLean Hospital and Massachusetts General Hospital. For the MDD studies, the local ethics boards were University of California Los Angeles (PDC), University of Kansas Medical Center (Kansas Musical Depression study) and the multi-profile clinic Pretor/International Institute of Psychology and Psychotherapy (Novosibirsk, Russia) (Russia fMRI Depression study)]. Based on the University of Liverpool guidelines and the NDA (from which data were obtained), ethics approval for analysing the present data were not required.

Note that full information on the approval of the study protocol must also be provided in the manuscript.

Field-specific reporting

Please select the one below that is the best fit for your research. If you are not sure, read the appropriate sections before making your selection.

Life sciences

Behavioural & social sciences

Ecological, evolutionary & environmental sciences

For a reference copy of the document with all sections, see nature.com/documents/nr-reporting-summary-flat.pdf

Life sciences study design

All studies must disclose on these points even when the disclosure is negative.

Sample size	We used the maximum number of participants with complete data on all variables of interest. For the ABCD, HCP-A, PDC, HCP-EP, we used only the data recommended for inclusion by the respective study teams. This information is available in all the data packages available for download. For the OpenNeuro MDD datasets, the detailed data quality control procedure is described in Segal et al. (2023)
Data exclusions	Due to insufficient participants to model race effects, only White ABCD and PDC participants were included in the analyses. For the other samples, who were predominantly White, we controlled for race using a White/non-White dummy coded variable.
Replication	To test the generalizability of our models, we used ten-fold cross-validation for our partial least squares and canonical correlation analyses. All the replication attempts were successful.
Randomization	This is an observational study which contains no experimental conditions that may require random assignment of participants to groups.
Blinding	This is an observational study which contains no experimental conditions (hence no need for blinding).

Reporting for specific materials, systems and methods

We require information from authors about some types of materials, experimental systems and methods used in many studies. Here, indicate whether each material, system or method listed is relevant to your study. If you are not sure if a list item applies to your research, read the appropriate section before selecting a response.

Materials & experimental systems		Methods	
n/a	Involved in the study	n/a	Involved in the study
<input checked="" type="checkbox"/>	Antibodies	<input checked="" type="checkbox"/>	ChIP-seq
<input checked="" type="checkbox"/>	Eukaryotic cell lines	<input checked="" type="checkbox"/>	Flow cytometry
<input checked="" type="checkbox"/>	Palaeontology and archaeology	<input type="checkbox"/>	MRI-based neuroimaging
<input checked="" type="checkbox"/>	Animals and other organisms		
<input checked="" type="checkbox"/>	Clinical data		
<input checked="" type="checkbox"/>	Dual use research of concern		

Magnetic resonance imaging

Experimental design

Design type	resting state fMRI, structural (VBM) MRI
Design specifications	<p>ABCD</p> <p>Four resting state fMRI scans (eyes open with passive crosshair viewing), lasting 20 minutes in total, were collected at each available time point (baseline/two-year follow-up) in order to ensure at least 8 minutes of low-motion data. Due to data availability, we used only 3 scans from each time point (6 resting state scans in total).</p> <p>HCP-A</p> <p>Four rfMRI scans (eyes open with passive crosshair viewing), lasting 26 minutes in total, were collected from all the participants. Two rfMRI scans were acquired with an anterior-to-posterior (AP) and the other two with a posterior-to-anterior (PA) phase encoding sequence. Because comparisons with the ABCD data were based on a single time point, we used only 2 of the 4 rfMRI scans in order to make scan duration comparable across samples. To facilitate potential future comparisons with the HCP-A task fMRI data on inhibitory control, which was collected with a PA phase encoding sequence, we only used the two resting scans acquired with a PA phase encoding sequence.</p> <p>Disorder-specific samples</p> <p>The resting state fMRI data for both the PDC (two resting state runs, each lasting approximately 6:30 minutes) and the HCP-EP (four resting state runs, each lasting approximately 5:30 minutes) were collected with the same parameters as for the HCP-A sample. Half of the runs for each sample were acquired with an anterior-to-posterior (AP) and the other half with a posterior-to-anterior (PA) phase encoding sequence.</p>
Behavioral performance measures	No behavioural performance measures were collected.

Acquisition

Imaging type(s)	resting state fMRI, structural (VBM) MRI	
Field strength	3T	
Sequence & imaging parameters	<p>Resting state fMRI ABCD: The fMRI data were acquired with a multiband EPI sequence (TR=800 ms, TE=30 ms, flip angle=52°, FOV = 216 mm, 90 x 90, matrix, 60 slices of 2.4 × 2.4 mm in-plane resolution, 2.4 mm thick, multiband acceleration factor of 6).</p> <p>HCP-A/PDC/HCP-EP The fMRI data were acquired with a multiband gradient-recalled (GRE) EPI sequence (TR=800 ms, TE=37 ms, flip angle=52°, FOV = 208 mm, 104 x 104 matrix, 72 oblique axial slices, 2 mm isotropic voxels, multiband acceleration factor of 8).</p> <p>Structural MRI: T1 image HCP-EP: 3D MPRAGE, TR = 2400ms, TE=2.22ms, flip angle = 8°, 208 sagittal slices, 0.8mm isotropic voxel size, FOV =256 x 240 x 166 mm, matrix = 320 x 300 x 208</p> <p>OpenNeuro MDD datasets (described in Segal et al., 2023): Kansas Musical Depression Study: 3D MPRAGE, TR = 2300, TE= 2.01 msec, flip angle = 9°, FOV = 256 mm, matrix = 256x256, 192 slices, slice thickness = 1 mm, Russia Depression fMRI: 3D turbo field echo, 1mm isotropic voxels</p>	
Area of acquisition	whole brain	
Diffusion MRI	<input type="checkbox"/> Used	<input checked="" type="checkbox"/> Not used

Preprocessing

Preprocessing software	<p>Resting State fMRI ABCD</p> <p>The minimal preprocessing pipeline was applied to the resting fMRI data from the ABCD study. This pipeline involved correction for head motion, spatial and gradient distortions, bias field removal, and co-registration of the functional images to the participant's T1-weighted structural image. We further applied the following steps: (1) elimination of initial volumes (8 volumes [Siemens, Philips], 5 volumes [GE DV25], 16 volumes [GE DV26] to allow the MR signal to reach steady state equilibrium, (2) linear regression-based removal of the mean time courses of cerebral white matter (WM), gray matter (GM), cerebrospinal fluid (CSF), as well as the quadratic trends and 24 motion terms (i.e., the six motion parameters, their first derivatives, and squares from the time course of each Schaefer parcel). Prior to being regressed, the motion terms had been filtered to eliminate signals within the respiratory effect range (i.e., .31-.43 Hz).</p> <p>HCP-A/PDC-HCP-EP</p> <p>Data were processed by applying the Generic fMRI Volume and Surface Processing Pipelines, multi-run independent component analysis (ICA) FIX denoising and multimodal surface matching registration. The Generic Volume Processing Pipeline accomplished removal of spatial and gradient distortions, correction for participant movement, bias field removal, spatial normalization to the standard Montreal Neurological Institute (MNI)-152 template (2 mm isotropic voxels), intensity normalization to a global mean and masking out of non-brain voxels. Subsequent temporal preprocessing steps involved weak high-pass temporal filtering with the goal of removing linear trends in the data. The Generic Surface Processing Pipeline registered the functional data into a standard grayordinate space by projecting the cortical gray matter into a registered surface mesh with a standard number of vertices (32k_fs_LR mesh) and projecting the subcortical data to a set of subcortical gray matter voxels. A small amount of spatial smoothing (2 mm full-width-at-half-maximum [FWHM]) was also applied to the functional data at this step. The ICA FIX denoising pipeline, which combines FSL's MELODIC with a more complex automated noise identifier ("FIX"), handled removal of artifacts (e.g., rigid/physiological motion-related) which had survived the Generic fMRI Volume Preprocessing step. Finally, the cleaned functional data were precisely aligned across participants through multimodal surface matching (MSM) registration</p> <p>Structural MRI</p> <p>To characterize disorder-specific profiles of cortical atrophy, we estimated regional gray matter volume (GMV) as this is one of the most frequently studied neural phenotypes in psychiatry. To this end, we used the CAT12 voxel-based morphometry (VBM) pipeline, which is included as an extension of Statistical Parametric Mapping software (SPM12, http://www.fil.ion.ucl.ac.uk/spm/software/spm12) in MATLAB v9.8. Briefly, the T1-weighted images underwent intensity correction and probability-based tissue class (grey matter, white matter, cerebrospinal fluid) segmentation. The segmented scans were normalized into standard Montreal Neurological Institute (MNI) space using the high-dimensional Diffeomorphic Anatomical Registration Exponentiated Lie Algebra (DARTEL). The images were bias-field corrected and modulated by the linear and nonlinear components of the Jacobian determinant obtained from the DARTEL deformation fields to obtain voxel-wise estimates of GMV. Lastly, the modulated segmented GM images were spatially smoothed with an 8mm (MDD maps) and 6 mm (psychosis) full width at half maximum (FWHM) Gaussian smoothing kernel.</p>	
Normalization	see data preprocessing above	
Normalization template	MNI standard	

Noise and artifact removal

see data preprocessing above

Volume censoring

see data preprocessing above

Statistical modeling & inference

Model type and settings

Multivariate (canonical correlation and partial least squares analyses) with 10-fold cross-validation, mediation analysis with bootstrapping

Effect(s) tested

Multivariate relationships of brain activity/network dynamics with (1) reproductive aging, pain, perceived hostility (2) receptor density, as well as disorder-specific atrophy and network dynamics maps

Specify type of analysis: Whole brain ROI-based BothStatistic type for inference
(See [Eklund et al. 2016](#))

Non-parametric inference

Correction

No multiple comparisons, hence no corrections necessary

Models & analysis

n/a Involved in the study

- Functional and/or effective connectivity
- Graph analysis
- Multivariate modeling or predictive analysis

Functional and/or effective connectivity

Pearson's r

Graph analysis

Subject-level, weighted multilayer graph (positive weights only); core measure: flexibility in nodal community assignments; Control measures (for effect specificity): network segregation/integration; participation coefficient based on negative vs positive weights

Multivariate modeling and predictive analysis

Partial least squares (PLS) canonical correlation analyses (CCA) with 10-fold cross-validation. PLS tested the correlation between whole-brain nodal graph metrics and reproductive aging, pain, perceived hostility. CCA tested the association of the brain maps identified with PLS and the receptor density, as well as disorder-specific graph metrics and atrophy maps.